Sustainable Food Technology

Accepted Manuscript

This article can be cited before page numbers have been issued, to do this please use: S. siddiqui, S. Jadaun and S. Bangar, *Sustainable Food Technol.*, 2025, DOI: 10.1039/D6FB00014B.

ROYAL SOCIETY OF CHEMISTRY

View Article Online
DOI: 10.1039/D6FB00014B

Sustainability Spotlight Statement

This research advances sustainable materials and food packaging technologies by valorizing rice straw, an underutilized agricultural residue, into high-performance all-cellulose nanocomposite films. Rice straw, which is often burned or discarded after harvest, is converted into a fully bio-based, biodegradable packaging material through cellulose extraction, regeneration, and nanofiber reinforcement. The study contributes to agricultural waste reduction while creating value-added materials for sustainable packaging applications. By enhancing mechanical strength, barrier performance, and biodegradability through cellulose nanofiber incorporation, this work supports the development of renewable alternatives to petroleum-based plastics. The research aligns with circular economy principles by promoting resource efficiency and closed-loop material use and demonstrates potential benefits for sustainable food packaging industries.

Development and Characterization of Rice Straw-Derived All-Cellulose Nanocomposite Films Reinforced with Cellulose Nanofibers Obtained via High-Intensity Ultrasonication and High-Shear Dispersion

View Article Online
DOI: 10.1039/D6FB00014B

Sadhana Jadaun[1], Saleem Siddiqui[1*], Sneh Punia Bangar[2*]

[1]Department of Life Science, Sharda School of Bioscience & Technology, Sharda University, Knowledge Park-III, Greater Noida, Uttar Pradesh, India.
[2]Department of Packaging and Graphic Media Science, Rochester Institute of Technology, Rochester, 14623 NY

*Corresponding authors: Saleem Siddiqui (saleem.siddiqui@sharda.ac.in) and Sneh Punia Bangar (spbipk@rit.edu; snehpunia69@gmail.com)

Abstract: Agricultural residue, rice straw, represents an underutilized source of cellulose with potential for value-added applications. In the present study, all-cellulose nanocomposite films were developed by incorporating cellulose nanofibers (CNFs) as reinforcing nanofillers within a regenerated cellulose matrix. The films were fabricated using a lithium chloride/N, N-dimethylacetamide (LiCl/DMAc) solvent system, providing a homogeneous dispersion of CNFs and facilitating strong interfacial interactions between the matrix and the nanofillers. The influence of CNF concentrations (0%, 3%, 5%, 7%, and 9%) on the morphology, barrier properties, crystallinity, mechanical performance, optical transparency, and thermal properties of the all-cellulose nanocomposite (ACNC) films was systematically evaluated.

The results indicated that tensile strength and modulus increased significantly with higher CNF concentrations, although the films exhibited brittleness at 9% CNF. FTIR analysis showed that the functional groups in the cellulose structure remained intact in the nanocomposites. The surface morphology of ACNCs studied through the Field Emission-Scanning Electron Microscopy (FE-SEM) showed the uniform distribution of CNF within the cellulose matrix.

The XRD analysis indicated that the incorporation of CNFs increased the crystallinity index of ACNC films, with CNF7 exhibiting the highest CI of 61.50%. The films were also characterized for their density, porosity, and moisture content, which were found to be influenced by CNF concentration. The water vapour transmission rate (WVTR) and oxygen transmission rate (OTR) of CNF7 were 44.7 ± 3.0 g/m²/day and 5.6 ± 0.8 cm³/m²/day, respectively, which were significantly lower than those of CNF0, likely due to increased tortuosity arising from CNF reinforcement. Although optical transmittance decreased with the incorporation of CNFs, the films retained sufficient transparency for food packaging applications. Thermal stability was also enhanced upon CNF addition, with the peak degradation temperature reaching 335.4 °C in CNF7. Biodegradability assessment using enzymatic degradation showed complete degradation of CNF7 within 75 days. Overall, the results highlight strong intermolecular interactions between CNFs and the cellulose matrix, leading to enhanced functional properties and demonstrating the potential of CNF-reinforced films for sustainable food packaging applications.

Keywords: all-cellulose nanocomposite, cellulose nanofibers, rice straw, tensile strength, biodegradability

1. Introduction

Rice is a major staple crop that feeds millions of more than half of the world's population, but its cultivation generates a significant amount of agricultural waste in the form of rice straw. Approximately 1 billion tonnes of rice straw are generated globally, with about 91% produced in Asia.[1] Among Asian countries, China is the largest producer of rice straw, followed by India, Indonesia, and Bangladesh.[2] The large-scale generation of rice straw presents a significant global management challenge, while also offering substantial opportunities for sustainability. However, a significant proportion of rice straw continues to be burned in countries such as Indonesia, India, Vietnam, China, and Pakistan.[3] In India, around 140 million tonnes of rice straw are generated annually, of which 84 million tonnes are burned in open fields due to the lack of efficient disposal and utilization practices.[1,4] Rice straw, with its high silica and lignin content, has poor nutritional value and limited use as animal fodder, causing large-scale accumulation on farms. Open field burning of straw releases harmful pollutants (CO_2, CO, NO_x, SO_x, VOCs, etc.), worsening air quality, contributing to respiratory diseases, and depleting soil nutrients.[5] Developing sustainable strategies to convert this agricultural residue into cellulose-based materials could provide an eco-friendly alternative for packaging applications, reducing environmental impact while supporting circular bioeconomy goals.

Cellulose is a linear biopolymer recognized for its biodegradability, non-toxicity, and high strength, which enhances its wide applicability in diverse fields. In nanoform, cellulose exists as cellulose nanocrystals (CNCs) and cellulose nanofibers (CNFs), which differ in structure and morphology. Owing to their higher aspect ratio, CNFs impart superior tensile strength and modulus to composites compared to CNCs, highlighting their potential in reinforcing packaging materials.[6] CNFs form an entangled, network-like structure through hydrogen bonding and van der Waals interactions, which contribute to their reinforcing ability in composite materials.[7,8] Their high surface area, aspect ratio, and mechanical strength, combined with biodegradability, renewability, and stability, make CNFs highly attractive as nanofillers for sustainable packaging materials. Growing concern over environmental impact has accelerated the search for sustainable packaging alternatives.[9] CNF-based materials, derived from renewable biomass, provide strong mechanical properties, improved barrier performance, and biodegradability, making them promising candidates for food packaging. Their use supports product preservation and freshness and aligns with global sustainability goals by reducing carbon footprint and environmental burden.[10]

All cellulose nanocomposites (ACNCs) are a subclass of green nanocomposites, where both the matrix and reinforcement phase are derived from cellulose.[11] This chemical compatibility enhances interfacial adhesion and stress transfer, resulting in superior mechanical strength and barrier performance. ACNC films, therefore, hold strong potential for application in fresh food packaging as sustainable, bio-based, and biodegradable alternatives.[12] ACNCs using microcrystalline cellulose and CNFs derived from wood pulp were fabricated by Guzmán-Puyol *et al.*[11] and observed significant improvements in mechanical strength and water vapor barrier properties, making them suitable for food packaging.

Similarly, Nascimento *et al.*[12] employed bacterial cellulose nanofibers as a matrix, reinforced with CNCs (0–5%), to produce ACNCs. The fabricated films exhibited high crystallinity, enhanced mechanical performance, improved water resistance, and reduced vapor permeability, thereby underscoring their potential for food packaging applications. In another study, Rader *et al.*[13] prepared ACNCS with Cellulose nanocrystals (CNCs) and Hydroxypropyl

cellulose (HPC). The film was transparent, with improved tensile strength and extensibility. The composites retained mechanical properties up to 75% relative humidity. Oxygen permeability decreased nearly tenfold at a 70% CNC concentration to levels comparable to those of PET, though water resistance remained limited, which indicated the need to optimize water barrier properties, important for food packaging. Yang *et al.*[14] demonstrated the development of all-cellulose nanocomposite films by mixing aqueous TEMPO-oxidized cellulose nanofibril dispersion obtained from softwood bleached kraft pulp with NaOH/urea/cellulose solutions prepared from cotton linter. The NaOH/urea/water solvent system used in their study represented an environmentally benign dissolution medium. The ACNCs have also been prepared from the components derived from various agricultural residues, including wheat straw [15], sugarcane bagasse[16], and corncobs[17].

The characteristic properties of cellulose and cellulose nanofibers depend on the biomass source of the fibers and the methods of their preparation, while the mechanical and barrier properties of the ACNC films prepared from them are affected by the concentration of nanofibers used as filler and the characteristics of the cellulose matrix[18, 15]. Rice straw, an abundantly available agricultural residue with associated disposal challenges, can be a promising low-cost raw material for the development of ACNCs. Despite extensive studies on the utilization of rice straw-derived CNF as a reinforcement agent in various polymer matrices [19,20,21], the studies investigating the combined utilization of rice straw-derived cellulose and CNFs within a single material system remain scarce and inconclusive. In our earlier work, cellulose was isolated from rice straw via alkali extraction, and the CNFs were prepared using an ultrasonication-assisted extraction technique coupled with high-shear dispersion[22]. In the present study, the ACNC films were developed from rice-straw-derived cellulose and various concentrations of CNFs, and the films were comprehensively characterized for their mechanical, barrier, optical, thermal, and biodegradation properties, considering their potential use in food packaging within a circular economy framework.

Experimental

2.1 Materials

Rice straw as obtained from the Experimental Agricultural Farm, Department of Agriculture, Sharda University, Greater Noida, India. Further, it was properly washed with deionized water and dried in a hot air oven at 40 ºC for 24 h. It was then cut manually into smaller sizes and stored properly in airtight polyethylene bags at ambient conditions for further investigation. Chemicals used in the study included Sodium hydroxide (NaOH), Sodium chlorite ($NaClO_2$), Sodium chloride (NaCl), and N, N-Dimethylacetamide (DMAc), which were purchased from Thermo Fischer India, and Lithium chloride (LiCl) was purchased from Loba Chemie Pvt Ltd., India.

2.2 Isolation of CNFs

Cellulose nanofibers (CNFs) were isolated following the procedure described in our previous work, Jadaun *et al.*[22] In brief, rice straw of short length of 4-5 cm was immersed in hot deionized water for 1 h and subjected to continuous stirring for an additional hour. Afterward, the straw was thoroughly washed with deionized water and dried overnight at 40 ºC in a hot air oven. The dried straw was then finely ground using a RETSCH Knife Mill Grindomix GM300 (Fischer Scientific) and sieved through a 60-mesh sieve. The ground straw was alkali-treated

View Article Online
DOI: 10.1039/D5FB00014B

with 12% NaOH at 121 ºC for 1 h. After treatment, the alkali-treated residue was washed repeatedly with deionized water to obtain a neutral pH and then dried in an oven at 50 °C overnight. Next, bleaching was performed using 10% acetified sodium chlorite (pH 3-5, adjusted with acetic acid) at 70 °C for 1 h. This process was repeated five times to effectively remove lignin. The resulting bleached fibers were filtered thoroughly with deionized water to obtain a neutral pH and then dried overnight at 50 ºC in a hot air oven to obtain purified cellulose.

A 0.1% cellulose fiber suspension was prepared by dispersing dried cellulose fibers in deionized water under continuous stirring. The dispersion was homogenized using IKA T18 Digital ULTRA-TURRAX at 17000 rpm for 2 h, with 10 min intermittent intervals. Subsequently, 60 ml of homogenized suspension was subjected to a high-intensity probe sonicator (VCX 750, Sonics and Materials Inc., USA) at 80% amplitude and 20 kHz frequency for 2h using a 13 mm probe. The resulting CNFs were freeze-dried and stored for further analysis.

2.3 Development of All-Cellulose Nanocomposite Films

A predetermined amount of cellulose was activated in 100 ml of *N, N*- dimethylacetamide (DMAc) at 80 ºC for 1 h under continuous stirring. After activation, 8 g of LiCl was added to the solution, and stirring was constant at 80 ºC for an additional 2 h. Subsequently, the temperature was lowered to 40 °C, and stirring was continued overnight to form transparent solutions. To assess the effect of CNF incorporation, varying concentrations of CNF, viz., 3.0%, 5.0%, 7.0%, and 9.0%, denoted as CNF3, CNF5, CNF7, and CNF9, respectively, were incorporated. CNFs were incorporated into this solution by adding a predetermined amount of CNF suspension under continuous stirring at 60 °C for 90 min to achieve uniform dispersion. The resulting solutions were stored under refrigeration to ensure consistency. A control sample (CNF0) was prepared using only cellulose, without any CNF. The prepared viscous solution was then cast on the Petri dishes and air-dried overnight to form a gel. These gels were then immersed in deionized water, with the solvent replaced every 2 hours for the complete removal of the DMAc/LiCl. The purified gels were transferred onto silicon mats and affixed to the glass plates using binder clips to avoid shrinkage. The films were subsequently left to air dry at room temperature.

2.4 Characterization

2.4.1 Chemical composition and Yield of cellulose

The chemical composition of the raw material, including cellulose, hemicellulose, and lignin, was determined before alkali and bleaching treatments. The analysis was performed using a slightly adapted Van Soest and Wine method[23], with modifications based on the procedure described by Pradhan and Bhatia[24], as detailed in our previous work [22]. In order to investigate the efficiency of alkaline and bleaching treatment in removing amorphous parts, the yield of cellulose was determined via the gravimetric method. The yield of extracted cellulose after these treatments was calculated using the formula given in equation (1):

$$\text{Yield (\%)} = \text{Final weight g} \div \text{Initial weight (g)} \times 100 \quad (1)$$

2.4.2 Sedimentation stability and Characterization of CNF

View Article Online
DOI: 10.1039/D5FB00014B

A cellulose suspension (1% w/w) was prepared in distilled water and subjected to high-shear dispersion followed by high-intensity ultrasonication, as described in our previous work[22]. The sedimentation stability of the resulting CNF suspension was evaluated by visual observation over time. The presence of nanofiber and diameter of CNFs were confirmed by FE-SEM, whereas parameters such as crystallinity, chemical composition, zeta potential, and thermal degradation behaviour were analysed by XRD, FTIR, zeta potential analyzer, and TGA as per the methodology described in Jadaun *et al.*[22]

2.4.3 Viscosity-average degree of polymerisation (DP_v) and molecular weight (M_w)

Viscometric analysis of the Molecular weight (M_w) and viscosity-average degree of polymerisation (DP_v) of samples was conducted according to the procedure described in previous studies by Kadivar *et al.*[25] and Maraghechi *et al.*[26], respectively, using a Cannon–Fenske viscometer and LiCl/DMAc solvent**.** Initially, bleached cellulose fibers, CNFs, and cellulose-CNFs solutions were prepared in 8% LiCl/DMAc solvent system under constant stirring speed to obtain a uniform solution.

Using LiCl/DMAc as the solvent, the solvent efflux time of the solvent and each solution was measured at 25 °C to determine intrinsic viscosity. From which, reduced viscosities of each solution (0.95, 1.15, 1.5, 1.85, and 3 (mg/cm^3)) were determined according to Hao *et al.*[27] using the equation (2) given below:

$$\eta_{red} = \frac{t - t_0}{c t_0} \quad (2)$$

where t_0 denotes the solvent efflux time, t is the efflux time of the solution, and c represents the cellulose solution concentration (g/cm^3).

The intrinsic viscosities were obtained by linear extrapolation of reduced viscosity versus concentration to zero concentration. From the intrinsic viscosity [η] of the samples, the corresponding values of the molecular weight were obtained by applying the Mark-Houwink-Sakurada equation (3):

$$[\eta] = K M_w^{\alpha} \, (cm^3 \, / g) \quad (3)$$

where the two empirical constants used were K = 1.278 × 10^{-4} and α = 1.19 (McCormick *et al.*[28]) for the LiCl/DMAc solvent system.

For the determination of Viscosity-average degree of polymerisation (DP_v), the relation between the intrinsic viscosity (η) with Viscosity-average degree of polymerisation (DP_v) established through the Mark-Houwink equation was used, as depicted in equation (4):

$$[\eta] = K \, (DP_v)^{\alpha} \quad (4)$$

2.4.4 Field Emission- Scanning Electron Microscopy (FE-SEM)

The surface morphology of pure cellulose film (CNF0) and ACNC films was observed using FE-SEM (JSM-7610F Plus JEOL, Japan) at an accelerating voltage of 15 kV at magnifications of 8,000x and 10,000x. Prior to imaging, film samples were affixed to aluminium stubs using double-sided conductive carbon tape. Using a sputter coater (DII-29030SCTR Smart Coater JEOL, Japan), samples were sputter-coated with a thin conductive/gold layer at 5nm/min to enhance conductivity.

2.4.5 Fourier Transform Infrared Spectroscopy (FT-IR)

The functional groups of the film samples were identified by FTIR (Agilent Cary 630 FTIR, USA) equipped with an Attenuated Total Reflectance (ATR) unit. Spectral data were recorded

View Article Online
DOI: 10.1039/D6FB00014B

over the range 4000 – 400 cm^{-1}, with each sample scanned 32 times at a spectral resolution of 2 cm^{-1}.

2.4.6 XRD analysis

XRD patterns of all the films were recorded using an X-ray diffractometer (SmartLab 3kW/ Rigaku) equipped with Cu Kα radiation (λ=1.54 Å). Scans were performed over a 2θ range of 5-90° at an accelerating voltage of 40 kV with a current of 40 mA. The films were mounted in a sample holder, and measurements were carried out in a static configuration. The XRD data were analyzed using Origin Pro 2026 (64-bit) software. The crystallinity index (CI) was calculated using the peak height method proposed by Segal *et al.*[29]

$$CI\ (\%) = \left(\frac{I_{002} - I_{am}}{I_{002}}\right) \times 100 \quad (5)$$

where I_{002} corresponds to the peak intensity of the (002) crystalline plane and I_{am} represent the minimum intensity located in the amorphous region between (002) and (001) peaks.

2.4.7 Moisture content

The moisture content of the films was obtained using the gravimetric method. Film specimens (2×2 cm^2) were initially weighed (M_o) and kept at 23 °C and 50% relative humidity (RH) until a constant weight was achieved (M_f). The moisture content was determined using the formula given below:

$$Moisture\ content = \frac{(M_o - M_f)}{M_o} \times 100\% \quad (6)$$

2.4.8 Density and Porosity

The thickness of each film was measured at 8 randomly selected points per film using a digital micrometer (Model 293-240-30, Mitutoyo Corporation, Japan) to the nearest 0.001 mm. The mean value of these measurements was calculated to determine the overall thickness of each film.

The density of the films (ρ_s) was determined by dividing the dry mass of the film by its geometric dimensions[30,31] as presented in equation (7) below.

$$\rho_s = \frac{m}{A \times \delta} \quad (7)$$

where m represents the dry mass of the sample (g), A denotes the surface area of the films (2 ×2 cm^2), and δ corresponds to the thickness (cm) of the film.

The porosity (ε) was assessed based on the previously reported gravimetric method by Liang *et al.*[32] using the following equation (8) given as:

$$\varepsilon\ (\%) = \left(1 - \frac{\rho_s}{\rho_c}\right) \times 100 \quad (8)$$

where ρ_s indicate the density of the film (g/cm^3) and ρ_c is the density of the cellulose ($\rho_c = 1.5\ g/cm^3$;(Yang *et al.*[33]) respectively.

2.4.9 Mechanical properties

The mechanical properties (Tensile strength, Elongation at break, and Tensile modulus) were tested using a Universal Testing Machine (Zwick Roell, Germany, Static UTM Z010). Film strips were cut into 55 mm × 10 mm in length and width with a tensile rate of 5 mm/min at room temperature.

2.4.10 Water Vapour Transmission Rate (WVTR)

Water vapour transmission rate (WVTR) was measured using a gravimetric method according to the modified method of the ASTM E96/E96 M-16, as described by Souza *et al.*[34] Initially, films were cut into circular size and sealed onto a glass vial with a diameter of 6.18 mm containing anhydrous calcium chloride desiccant. These sealed vials were kept in a desiccator filled with a saturated NaCl solution (maintained at 25 °C and 75% relative humidity) at the bottom part. The desiccator was then sealed properly to avoid the passage of air inside the desiccator. The weight of each vial was recorded at the start (time zero) and subsequently every 24 h for 3 days. Water vapor permeated through the films and was absorbed by the desiccant; evaluations were determined by measuring the weight gain per unit area. The water vapor transmission rate (WVTR) was calculated using equation (9).

$$WVTR = \frac{G}{tA} \quad (9)$$

where G is the weight change in g, t is the time in h, and A is the effective area of the film in m^2.

To determine Water Vapour Permeability (WVP), in g Pa^{-1} m^{-1} s^{-1}, the following equation (10) can be employed:

$$\mathrm{WVP} = \frac{WVTR \times L}{\Delta P} \quad (10)$$

where L is the thickness of the film in meters, and ΔP is the partial pressure difference of water vapor across the film in Pascals.

2.4.11 Oxygen Transmission Rate

The Oxygen Transmission rate **(**OTR) of the control film and ACNC films was determined with an automated Oxygen Transmission Rate Test System (PERME® OX2/230 Labthink, China). According to ASTM D3985, the measurements were carried out using high-purity oxygen (99.999%) at 38 °C and 90% relative humidity. Each sample had a test area of 65 cm^2.

1.4.12 Color properties and Optical transmittance

The color properties (L^*, a^*, b^*) of the developed films were measured using a Chroma meter, CR-400 (Konica Minolta Optics, Inc., Japan) under CIE 1931 2° standard observer with illuminant C/D65 conditions. The L^*(lightness/brightness), a^* (redness/greenness), and b^* (yellowness/blueness) were recorded using this device. The chroma (C^*) and hue angle (H°) values were calculated according to Equations (11 & 12), as mentioned by Sganzerla *et al.* [35]:

$$C^* = \sqrt{a^{*2} + b^{*2}} \quad (11)$$

$$H^o = \tan^{-1}\frac{b^*}{a^*} \quad (12)$$

View Article Online
DOI: 10.1039/D6FB00014B

The total color difference (ΔE_{ab}) of the films relative to the control (taken as control) was calculated using Eq. (13).

$$\Delta E_{ab} = \sqrt{(\Delta L^*)^2 + (\Delta a^*)^2 + (\Delta b^*)^2} \quad (13)$$

Where, $\Delta L^* = L^*_{standard} - L^*_{sample}$, $\Delta a^* = a^*_{standard} - a^*_{sample}$, $\Delta b^* = b^*_{standard} - b^*_{sample}$

The optical transmittance (Tr) of ACNC films was determined with a double–beam UV–Vis spectrophotometer (UV-Vis Spectrophotometer, LMSP-UV1900S, Labman Scientific Instruments Pvt. Ltd., Chennai) at the wavelength of 800 nm, as per the procedure explained by Zhao *et al*.[36] The average thickness of the composite films was about 40 µm. The transmission spectra were acquired using air as a blank.

2.4.13 Thermal gravimetric analysis (TGA)

The thermal stability and thermodegradation behavior were analyzed using a thermal gravimetric analyzer (TGA 2 STARe system, Mettler Toledo, Switzerland). The sample of~5 mg or less was placed in the crucible and heated in the temperature range of 30 to 600 °C at a heating rate of 10°C/min under a nitrogen atmosphere. Thermogravimetric analysis (TGA) provided the information about the overall weight loss as a function of time/temperature, while Derivative Thermogravimetry (DTG) represented the first derivative curve, which showed the rate of mass change with respect to temperature and time.

2.4.14 Biodegradability

The biodegradability of all the films was assessed using the technique explained by Kim *et al*.[37] Films were cut into 3 × 3 cm² specimens, weighed, and immersed in reagent bottles containing a cellulose solution (3 mg/mL in PBS, pH 6.0). The reagent bottles were maintained in an incubator at 37 °C and monitored for 75 days. Additionally, ACNC films were tested in distilled water without the cellulase enzyme as a negative control. At 15-day intervals, films were removed from cellulase solution, washed with DI water to remove residual enzyme, dried in a hot air oven at 40 ºC, and weighed. The dry weight was recorded, and the percentage weight loss was calculated using equation (14) given below:

$$Weight\ loss\ (\%) = \frac{W_0 - W_1}{W_0} \times 100 \quad (14)$$

where W_0 represents the initial weight of a specimen, and W_1 is the weight of the specimen on a given day of sampling.

2.5 Statistical analysis

Experiments were conducted in triplicate, and values are presented as mean ± standard deviation (SD). Data was analysed by one-way analysis of variance (ANOVA) under a completely randomized design (CRD). The sample mean values were compared using Fisher's least significant difference (LSD) test at a significant level of 0.05 ($p \leq 0.05$). The obtained instrumental data were interpreted and analysed using Origin Pro SR1 software.

3. Results and discussion

View Article Online
DOI: 10.1039/D6FB00014B

3.1 Chemical composition and yield of cellulose

The cell wall of natural fibers is composed of reinforced cellulose microfibrils embedded in the amorphous matrix made up of hemicellulose and lignin. The complex intermolecular interactions and structural arrangement of cellulose, hemicellulose, and lignin provide the natural recalcitrance of lignocellulosic biomass. To overcome this recalcitrance and isolate cellulose fibers, chemical treatment, i.e., alkaline treatment (12% NaOH) followed by bleaching (10 % acidified $NaClO_2$), was performed according to the protocol described in our earlier work, Jadaun *et al.*[22] As has already been reported in that communication, the hemicellulose and lignin in rice straw were 19.33±0.03% and 10.03±0.05%, respectively. After alkali treatment, the contents of hemicellulose and lignin were reduced to 6.26±0.01% and 2.23±0.02%, respectively, whereas cellulose percentage in the residue was increased from 35.03±0.15% to 78.70±0.1%. This enhancement reflected that alkali treatment partially disrupted the complex matrix through the cleavage of ester linkages in lignin-hemicellulose, which led to the dissolution of hemicelluloses. Consequently, hemicellulose and lignin were partially removed, and a further bleaching process eliminated insoluble lignin along with residual hemicellulose from the rice straw pulp, which enhanced cellulose content to 92.08±0.1%. It indicated that the combined treatments efficiently removed non-cellulosic components, resulting in the extraction of purified cellulose fibers, with cellulose yield approximately 42%, which was found to be comparable to the values reported in the literature for garlic stalk, corncob, and giant cane cut-up.[38]

3.2 Sedimentation stability and Characterization of CNF

Fig. 1 illustrates the sedimentation behaviour of the 1% (w/w) CNF suspension after high shear dispersion (HSD), and after combined treatment of high intensity ultrasonication (HIU) and HSD. After one hour of HSD, the suspension was observed to be partially translucent in appearance, with noticeable sedimentation at the bottom of the vial (Fig. 1a). When HSD was followed by HIU, the cellulose suspension became homogenous, stable, and exhibited slight opalescence rather than full transparency (Fig. 1b). Wang *et al.*[39] reported high transparency for low (0.1%) concentration levels of cellulose, while at high concentration levels, the suspension appeared to be turbid because of the increased fiber content. The effectiveness of the combined treatment could be due to the effect of HSD that partially disrupted the hydrogen bonding among the microfibers and loosened the amorphous region, while HIU treatment resulted in nano-fibrillation by cavitation effect. The nanofibrillation is also evident in the FESEM image (Fig. 1c), where a web-like structure was observed with a nanoscale fibrillar network. It has already been communicated in our earlier communication[22] that the individual fibrils exhibited an average diameter of 34.2 nm and length of 1765.9 ± 42.1 nm, a mean zeta potential of -12 mV, and the maximum degradation temperature of 329 °C. The crystallinity index (CI) of CNFs was 80.5%, which was significantly improved as compared to cellulose after NaOH (CI: 50%) and $NaClO_2$ bleaching (CI: 68%) treatments. These reported results for optical appearance, nanoscale dimension, fiber morphology, and thermal stability confirmed that the prepared fibers were CNFs rather than MFC.

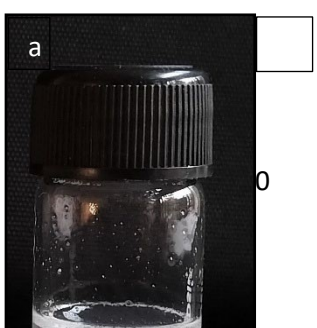

View Article Online
DOI: 10.1039/D6FB00014B

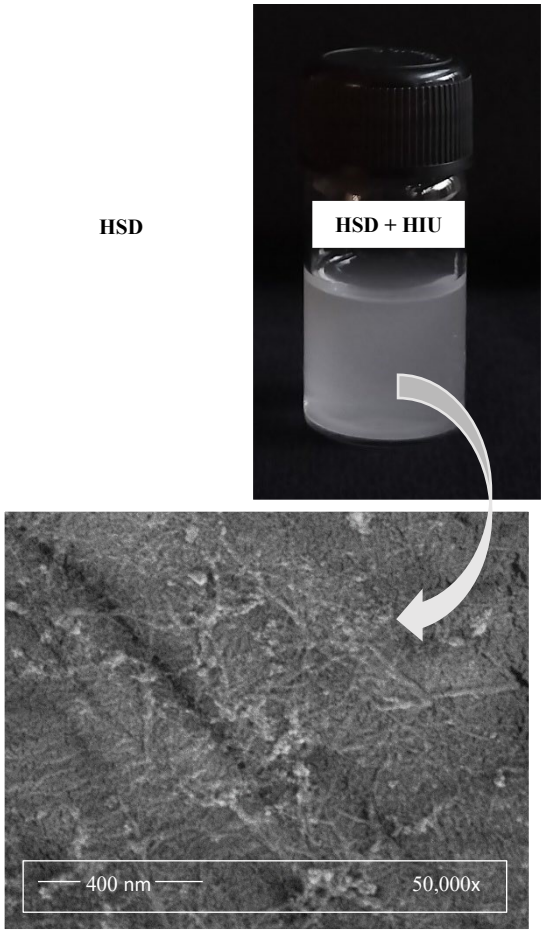

Fig. 1. (a) CNF dispersion after HSD, showing partial sedimentation, (b) CNF dispersion obtained after combined treatment of HSD and HIU, showing improved homogeneity and stability, and (c) FESEM-image of CNFs after HSD + HIU treatment, revealing a nanofibrous surface morphology of fibers observed at a magnification of 50,000x

3.3 Homogeneity and visual appearance of the films

After the isolation of CNF, uniform and transparent CNF films were successfully fabricated via the DMAc/LiCl dissolution-regeneration method. Fig. 2 illustrates the overall procedure of nanocomposite film preparation from rice straw. The ACNC films developed through solution

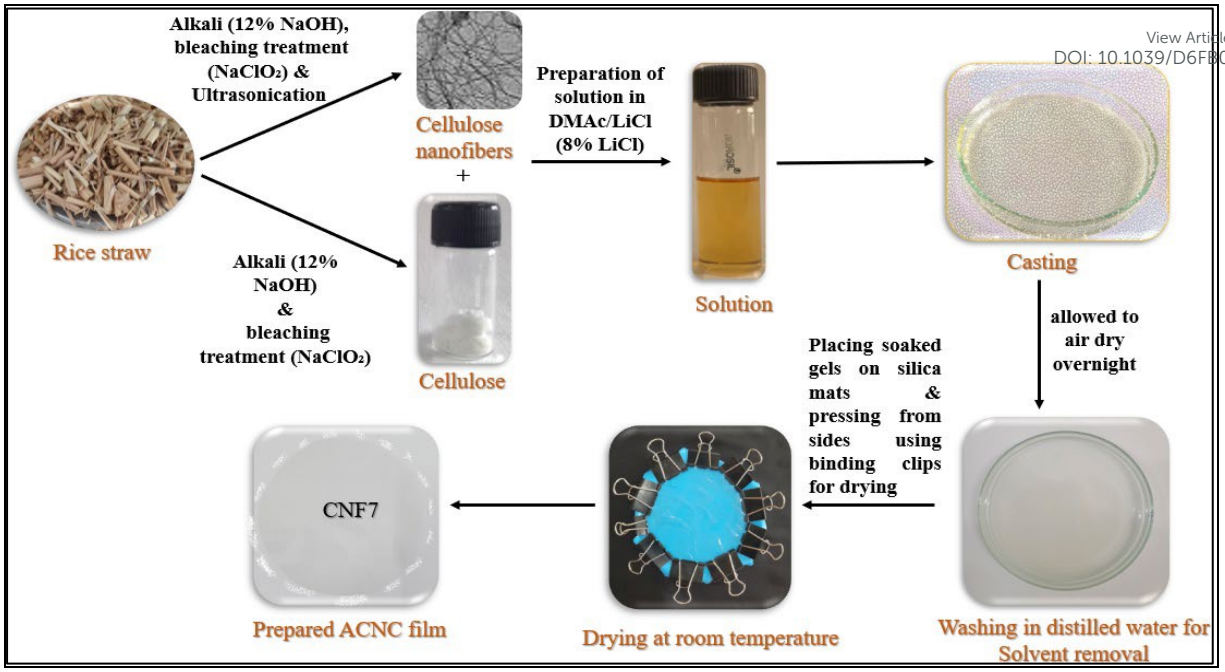

Fig. 2. An overview of the preparation of nanocomposite films from rice straw. The extracted cellulose and CNFs from rice straw were introduced in DMAc/LiCl to achieve cellulose dissolution and CNF dispersion, followed by casting. The prepared gels were washed and dried at room temperature to obtain the ACNC films.

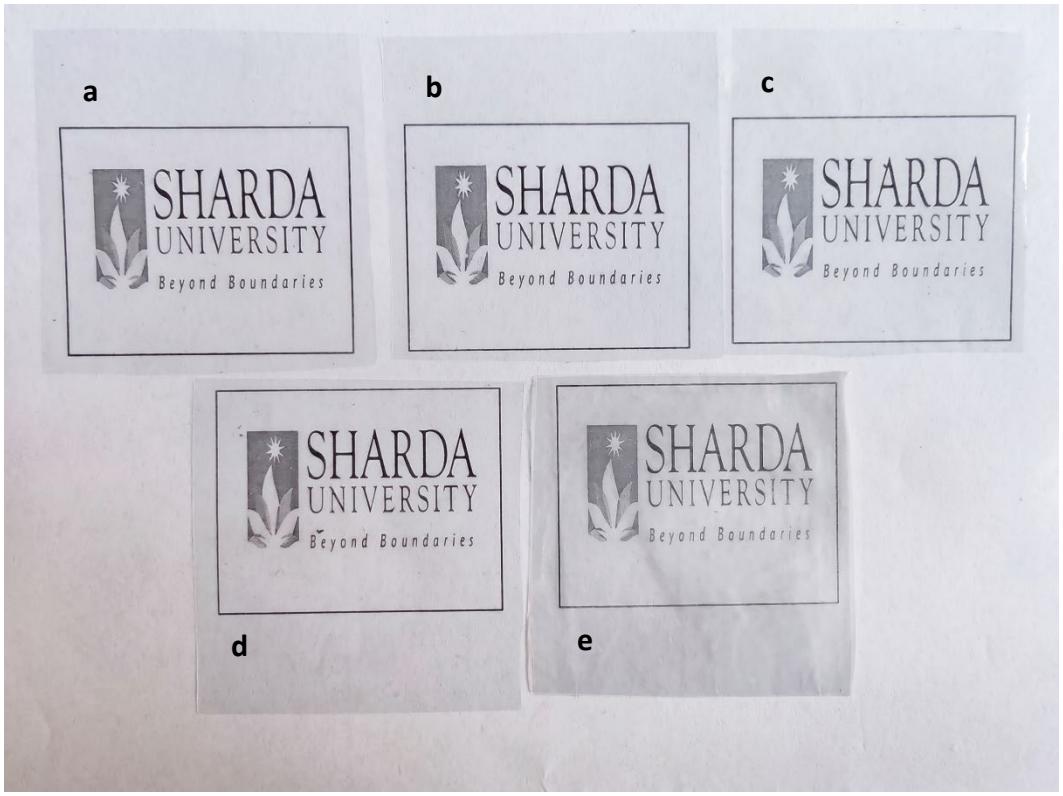

Fig. 3. Digital images of ACNC films (a) CNF0, (b) CNF3, (c) CNF5, (d) CNF7, and (e) CNF9 showing clarity of the text and images through the film samples.

casting, as shown in Fig. 3, illustrate the visual appearance of the films at different CNF concentrations. All films were uniform and smooth throughout, as can be observed from these images, except the CNF9 film, which showed relatively decreased transparency and rigidity due to the presence of agglomerated CNFs as observed by FE-SEM analysis (see Fig. 4). These visual observations aligned with the UV-Vis results, which quantitatively demonstrated the transparency differences. However, the solution appeared yellowish in color (as shown in casting steps in Fig. 2) when first spread onto the mold, but became transparent after solvent removal. The control film (CNF0), containing only cellulose, was flexible, whereas adding CNF significantly improved the mechanical strength of the films. The ACNCs could be rolled and folded without breaking and remained stable without flaking at room temperature. No visible traces of undissolved CNF were seen on the surface (consistent with FE-SEM results), suggesting uniform dispersion within the matrix. After drying, all films could be easily peeled from the casting frame without damage.

3.4 Viscosity average degree of polymerisation and molecular weight

The molecular weight (M_w) of cellulose affects the properties of cellulose-based materials (e.g., films), in terms of mechanical properties and crystallisation behaviour.[40] It forms the basis for understanding the structure-property relationship of cellulose-based materials, as M_w reflects the average chain length of cellulose molecules, which defines the dissolution behaviour[41] and chain entanglement[42] in LiCl/DMAc. The viscosity-average degree of polymerization (DP_v) is directly related to cellulose chain length and is measured from intrinsic viscosity measurements that reflect the hydrodynamic dimensions of cellulose chains in solution. The intrinsic viscosity (η), molecular weight (M_w), and viscosity average degree of polymerisation (DP_v) of bleached cellulose fibers, CNF, and the cellulose-CNF solutions are summarized in Table 1. However, it was not possible to determine the viscosity-average degree of polymerization of the cellulose after NaOH pulping because the pulp after alkali treatment was not purified cellulose and could not be dissolved in DMAc/LiCl due to the presence of lignin.

Table 1. Polymer characteristics of treated fibers

Sample	[η] (mL·g^{-1})	M_w (×10^5 g·mol^{-1})	DP_v (×10^3)
Bleached Cellulose fibers (rice straw)	1023 ± 3.0^a	6.32 ± 0.02^a	3.90 ± 0.01^a
CNF	958 ± 2.6^e	5.98 ± 0.03^c	3.69± 0.01^c
Cellulose + CNF (3% CNF)	994 ± 1.0^d	6.18 ± 0.02^b	3.81± 0.03^b
Cellulose + CNF (5% CNF)	997 ± 2.0^c	6.19 ± 0.03^b	3.82± 0.02^b
Cellulose + CNF (7% CNF)	998 ± 2.0^c	6.19 ± 0.01^b	3.82± 0.03^b
Cellulose + CNF (9% CNF)	1002 ± 1.7^b	6.21 ± 0.02^b	3.83± 0.01^b

η-intrinsic viscosity, M_w -Molecular weight, and DP_v-Viscosity degree of polymerisation. Mean values with different superscript letters in the same column are significantly different ($p \leq 0.05$).

The intrinsic viscosity of the bleached cellulose fibers was 1023 ± 3.0 mL·g^{-1}, which provided M_w of 6.32 ×10^5 g·mol^{-1} and DP_v of 3.90×10^3. The intrinsic viscosity of the CNF was significantly decreased to 958 ± 2.6 mL·g^{-1} (M_w=5.98×10^{5}g·mol^{-1}; DP_v=3.69×10^3) after mechanical fibrillation. The observation implied that ultrasonication caused a decrease in the length of cellulose fibres due to chain scission by cleavage of the glycosidic bonds. A similar

View Article Online
DOI: 10.1039/D5FB00014B

reduction in degree of polymerisation after ultrasonic treatment or homogenisation has been reported in previous studies by Dilamian and Noroozi[43], and Du *et al.*[44]. However, when CNFs were mixed with cellulose in LiCl/DMAc, the intrinsic viscosity values were found to be increased relative to CNF alone (994 ± 1.0-1002 ± 1.7 $mL \cdot g^{-1}$), which corresponded to M_w values of 6.18-6.21×10^5 $g \cdot mol^{-1}$ and DP_v values of 3.81-3.83×10^3. The absolute M_w values depend on the solvent-specific Mark-Houwink constant (K,α). The M_w values with LiCl/DMAc system suggested that cellulose did not undergo significant degradation during the dissolution process, as the solvent system is known to solubilize high molecular weight cellulose without degradation.[45,46] The relatively high M_w and DP_v values in the cellulose-CNF solutions demonstrated that the polymer chains remained sufficiently long to contribute to the entanglement-driven mechanical reinforcement, and to allow strong chain entanglement and network formation in the regenerated films. The slight decrease in M_w in CNF could be due to defibrillation that occurred during ultrasonication. The high molecular weight of the cellulose chains supported effective chain entanglement during regeneration, while increased CNF concentration introduced additional structural interactions within the cellulose matrix that may have resulted in improved mechanical performance in the ACNC films.

3.5 FE-SEM Analysis

Fig. 4 (a-e) presents the morphology of pure cellulose film (CNF0) and CNF reinforced nanocomposite films. The CNF0 (as shown in Fig. 4(a)) exhibited a smooth, dense, and uniform surface without visible defects. A similar successful film formation has been reported by Moreira *et al*.,[47] who attributed it to the strong intermolecular cohesion among cellulose chains. Incorporation of CNF did not significantly alter the surface morphology of the nanocomposite films (ACNCs) up to 7% CNF loading.

However, at 9% CNF (Fig. 4e), surface roughness became evident, likely caused by CNF agglomeration within the cellulose matrix. This behaviour suggested that higher CNF concentrations promoted aggregation due to strong intermolecular interactions, leading to non-homogeneous dispersion and potential deterioration of film properties.[48] Comparable findings were reported by Shazleen *et al*.[49] for CNF-reinforced PLA (Polylactic acid) nanocomposite films, where high CNF content impeded polymer chain mobility.

All films except CNF9 displayed compact, pore-free surfaces with no detectable surface irregularities, suggesting uniform dispersion and effective incorporation of CNFs into the matrix. The internal structure appeared dense and cohesive, without any visible traces of the original fibrous morphology of the nanofibers, suggesting that CNFs were well dispersed in the cellulose matrix during processing and subsequently underwent structural reorganization upon heating of the cellulose-CNF solution for the development of ACNCs. The absence of discrete CNF regions further confirmed that the films behaved as molecularly integrated systems rather than conventional fiber-reinforced composites, as evident in Fig. 4 (b, c,& d). Interestingly, the higher-magnification FE-SEM micrograph of the CNF7 film (Fig. 4e) revealed a finely textured surface, indicative of nanoscale features potentially associated with CNF residues. Overall, increasing the CNF concentration up to the optimum level of 7% preserved the compact morphology while enhancing internal structuring and surface uniformity.[50] This molecular-level reinforcement is likely responsible for the improved structural integrity, and uniformity observed in the nanocomposite films.

View Article Online
DOI: 10.1039/D6FB00014B

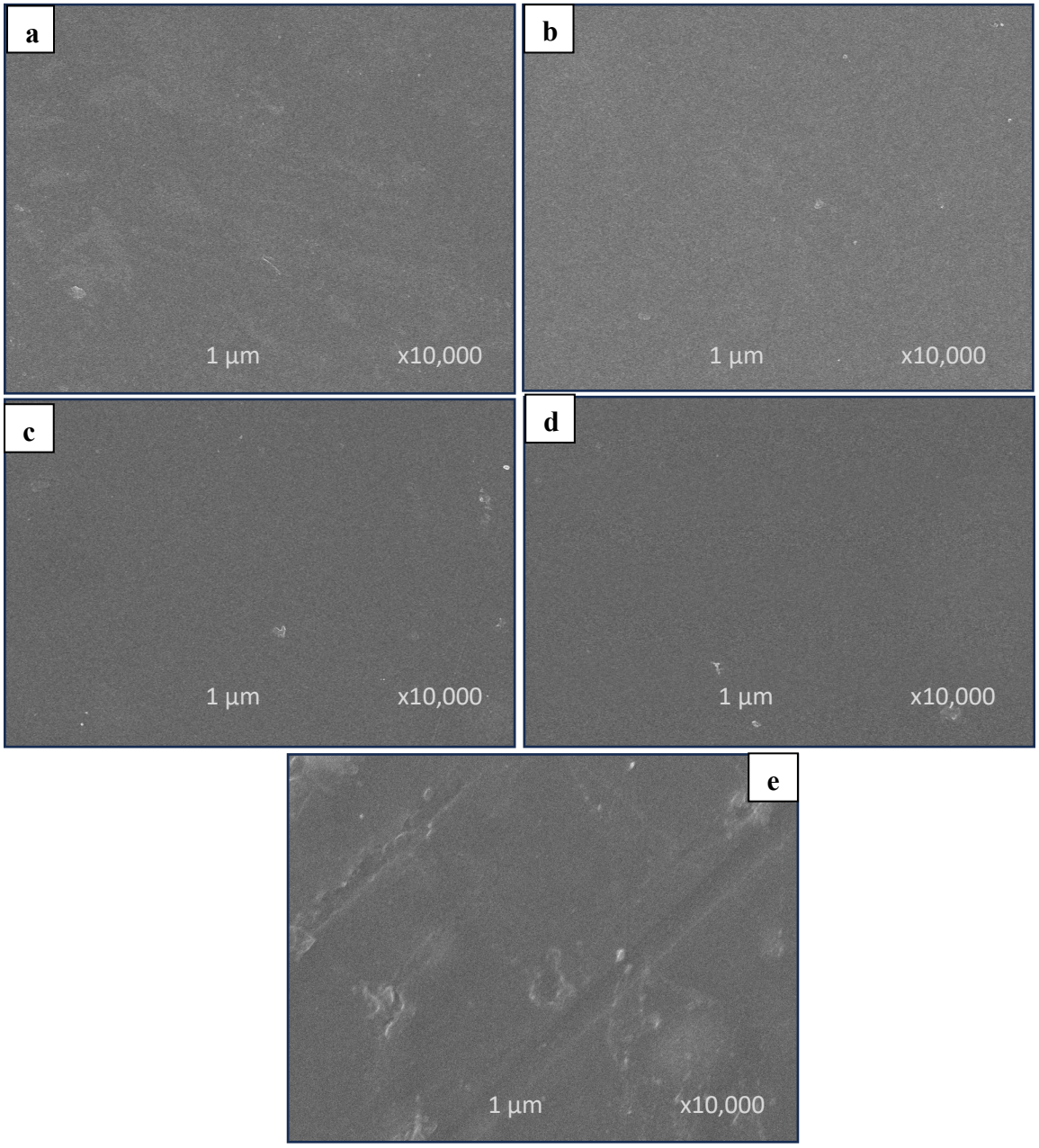

Fig. 4. FE-SEM images x 10,000 of CNF0 and ACNC films (a) CNF0, (b) CNF3, (c) CNF5, (d) CNF7, and (e) CNF9, showing smooth and dense surfaces of film samples from CNF0 to CNF7, while agglomeration was observed in CNF9.

3.6 Fourier transform infrared spectroscopy (FTIR)

FTIR analysis was performed to evaluate the influence of CNF concentration and the solution casting method on film structure (Fig. 5). In all samples, the broad dominant peaks observed around 3300 cm^{-1} corresponded to OH group stretching vibrations, indicating the presence of intra- and intermolecular hydrogen bonding within the cellulose structure.[51] Additionally, in the region of 2880 – 2900 cm^{-1}, C-H stretching vibrations were observed, corresponding to the primary functional groups of cellulose.

The intensity of the -OH band increased with CNF addition, indicating enhanced hydrogen bonding between the cellulose matrix and CNF. The region between 1629 cm^{-1} - 1640.0 cm^{-1} was ascribed to O−H bending vibrations of water molecules absorbed by the cellulose structure. The CH_2 bending vibrations of the pyranose ring were observed at 1423.8 cm^{-1} and 1428.06 cm^{-1}, reflecting the crystalline structure of cellulose.[52] The majority of distinctive bonds in the fingerprint region (800 -1500 cm^{-1}) of cellulose remain consistent in all spectra.[53] The C−O−C stretching vibration detected at peak 1155.5 cm^{-1} was found to be constant in all film samples.[54] Additionally, the CH deformation vibration was slightly shown at the peak of 1371.7 cm^{-1} in the spectra.[55] The prominent peaks at 1013.8 cm^{-1} and 1017.6 cm^{-1} were related to C-O vibration stretching in cellulose. The tiny peaks seen at 895.41 cm^{-1} and 898.3 cm^{-1} depicted the C-O-C stretching vibration of the β-glycosidic link in cellulose. This indicated that regardless of different processing treatments, the fundamental structure of cellulose remained intact throughout, and an increase in intensity validated the existence of intermolecular interaction and compatibility.

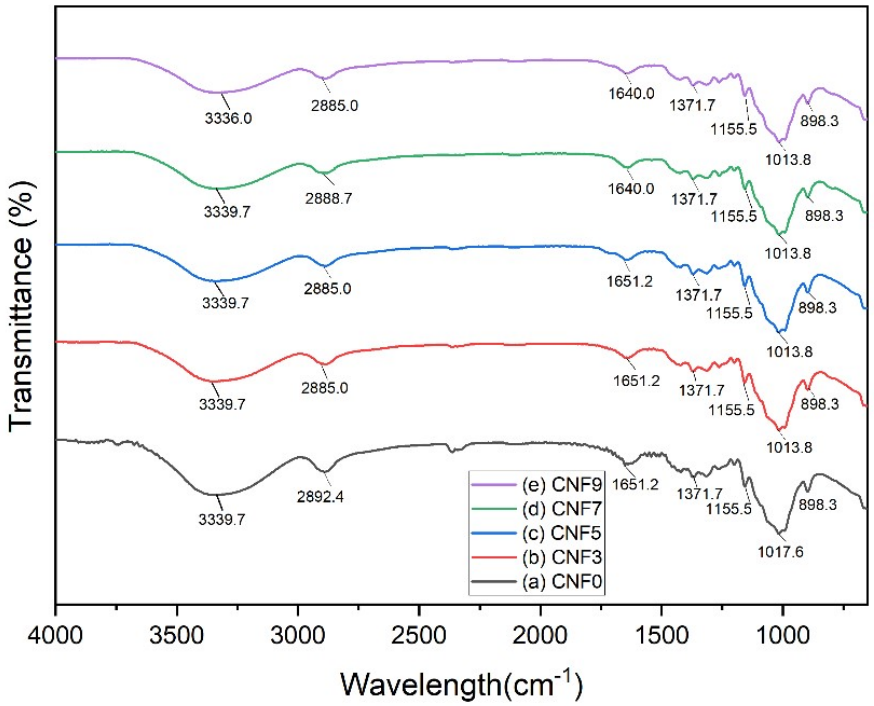

Fig. 5. FTIR spectra of (a) CNF0, (b) CNF3, (c) CNF5, (d) CNF7, and (e) CNF9 at different CNF concentrations.

3.7 Moisture content

Moisture content strongly influences the mechanical and barrier performance behaviour, particularly in hydrophilic polymers. The moisture of cellulose film without reinforcement was estimated to be 15.78 ± 0.08 % (Table 2) and was significantly higher than ACNC films ($p \leq 0.05$). With increasing CNF concentration, the moisture content of ACNC decreased markedly, with up to 63.6 % reduction in CNF7 relative to the control. However, the agglomeration in CNF9, as is evident in FESEM image (Fig. 4e), likely resulted in slightly higher moisture content in CNF9 as shown in Table 2. This decrease in moisture content with an increase in CNF could likely be due to the restricted space available for moisture because

of the interaction between CNF and cellulose matrix [56]. Faisal et al.[51] also reported that the moisture content in amylose films decreased by CNF incorporation due to the entanglement behaviour of CNF. Deepa et al.[57] and Kesari et al.[58] found that the interaction of CNF and polymer matrix led to a decreased number of active sites for water binding. The formation of a dense fibrous CNF network further limited water absorption and led to reduced moisture content.

Table 2. Structural properties and crystallinity of the films

Samples	Thickness (mm)	Moisture (%)	Density (g/cm^3)	Porosity (%)	CI (%)
CNF0	0.033 ± 0.003^{c}	15.78 ± 0.08^{a}	1.02 ± 0.03^{d}	31.82 ± 0.33^{a}	39.90
CNF3	0.038 ± 0.004^{b}	11.23 ± 0.03^{b}	1.12 ± 0.01^{c}	27.60 ± 0.21^{b}	51.02
CNF5	0.041 ± 0.002^{ab}	8.61 ± 0.08^{c}	1.20 ± 0.02^{b}	23.31 ± 0.23^{c}	50.00
CNF7	0.043 ± 0.002^{ab}	5.75 ± 0.05^{e}	1.25 ± 0.01^{a}	18.40 ± 0.19^{e}	61.50
CNF9	0.046 ± 0.003^{a}	6.12 ± 0.02^{d}	1.21 ± 0.04^{b}	22.50 ± 0.17^{d}	57.80

Values are represented as mean ± SD (n=3). Mean values with different superscript letters in the same column are significantly different ($p \leq 0.05$).

3.8 Thickness, Density, and Porosity

Determination of film thickness is pivotal, as it influences the density and barrier properties of the film. The measured thickness of the control and ACNC films ranged from 0.033± 0.003 to 0.046 ± 0.003 mm. There was a significant difference observed due to the incorporation of CNF in the matrix. The significant increase in thickness from CNF0 to CNF9 can be attributed to the higher CNF loading and enhanced intermolecular interactions caused by CNFs, which led to higher viscosity of the film-forming solution during the casting process. The results of thickness are similar to earlier findings reported for sugarcane bagasse-derived CNF-reinforced starch films prepared using the solvent casting method by Ribeiro et al.[59] For a nanocomposite film, density indicates the structural compactness, which depends on the arrangement of nanofillers and the packing of polymer chains. As given in Table 2, the density significantly increased with increasing CNF concentration, and ranged from 1.020 ± 0.03 to 1.21 ± 0.04 g/cm^3 among the film samples. Among all the samples, CNF0 had relatively low density, which could likely be due to its less compact microstructure and presence of microvoids throughout the film. Gashawtena *et al.*[60] reported that the presence of CNF reduced microvoids and formed denser structures. The incorporated CNF imparted a noticeable impact in the matrix by occupying the intermolecular spaces and strengthening H-bonding across the fibre network. In the present investigation, these interactions within the cellulose matrix might have resulted in the reduction of free space in the film, which led to a tightly packed structure with lower porosity.

The porosity of the films declined significantly with the increase in the CNF concentration, as presented in Table 2, with CNF7 showing a reduction of 42.17% compared to CNF0. This decrement is probably linked to the creation of a tighter and more highly interconnected microstructure owing to the hydrogen bonding and CNF network consolidation, which is prevalent in films prepared with nanocellulose[61]. Wakabayashi *et al.*[62] observed that the higher degree of fibrillation in nanocellulose films led to a significant decline in porosity, i.e., approximately 70% to 20%. The values of porosity obtained in the present study are relatively lower than those reported for hot-pressed CNF films made through natural drying[32], and for the cellulose acetate/lignin-rich CNF-based nanocomposite film.[63]

View Article Online
DOI: 10.1039/D6FB00014B

3.9 XRD (X-ray diffraction)

The XRD patterns of the fabricated ACNC films are presented in Fig. 6, and the corresponding crystallinity index (CI) values, determined using the Segal method, are summarized in Table 2. The dominant peaks at approximately 2θ = 14° and 20° were observed in all ACNC samples, indicating a polymorphic transformation from cellulose I to cellulose II, although a minor fraction of cellulose I was also present. This indicated that dissolution/regeneration of cellulose in DMAc/LiCl led to alteration of the cellulose I crystal structure, consistent with the observations made by Zhang *et al.*[64]. Table 2 displays a considerable difference in crystallinity index between the film with reinforcement and without reinforcement. The crystallinity index further increased with CNF concentration, which indicated the strong interaction between CNFs and the cellulose matrix. With an increase in CNF concentration (3-7%), diffraction spectra were found to be refined at the peak (002). This indicated that a crystalline ordered structure was formed inside the matrix, revealing the role of nanofibers as nucleating for in nanocomposites.[65,66] This enhancement is reflected in the increased CI from 39.9% in CNF0 to a maximum of 61.5% in CNF7, demonstrating that the presence of nanofibers induced the rise of crystallinity in nanocomposite films.[67] However, for CNF9, a lower CI compared to CNF7 indicated the beginning of agglomeration of nanofibers (revealed by FE-SEM images). This agglomeration may have led to a reduction in the internal order and resulted in lower crystallinity compared to CNF7. Similar CI values have been reported by Roy *et al.*[68] who demonstrated that nanocomposite films containing CNF/Zinc oxide, CNF/grapefruit seed extract, and CNF/Zinc oxide/grapefruit seed extract had CI values of 59.31%, 61.26%, and 60.45%, respectively. In contrast, Lal *et al*.[69] reported significantly lower CI values ranging from 9.3% -22.5% for tamarind seed polysaccharide films incorporated with 0.1-1% old corrugated box-derived CNF, which was found to be lower than the CI obtained in this study. The improved crystallinity obtained in this study is likely to influence the reinforcing ability of the nanoparticles, which is expected to enhance the mechanical and barrier properties of the composite films.[70]

Since no intact nanofibrous morphology was observed in FE-SEM images, the reinforcing effect may not be directly inferred from the microstructure observations. However, CI showed a systematic increase in crystallinity with the addition of CNF, indicating that although CNFs lost their original fibrous morphology in the LiCl/DMAc system, they acted as effective nucleation and ordering sites during cellulose regeneration[56]. The presence of CNFs promoted recrystallization and the formation of ordered crystalline domains during the regeneration process, which led to structure-induced reinforcement in the regenerated films.

View Article Online
DOI: 10.1039/D6FB00014B

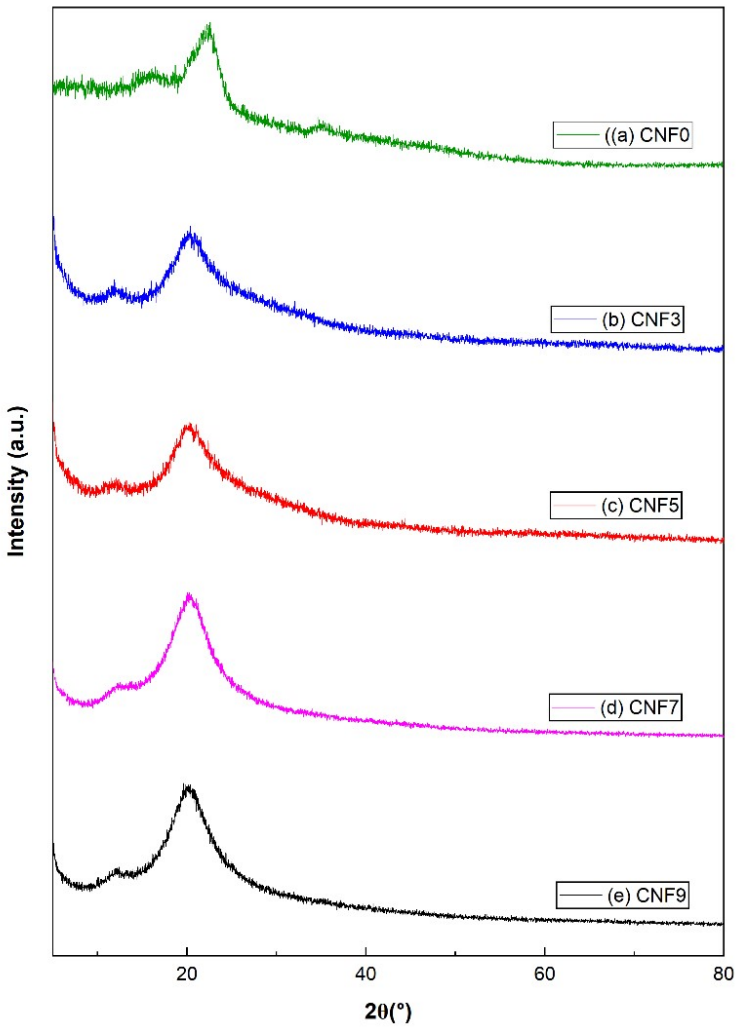

Fig. 6. XRD spectra of CNF0, CNF3, CNF5, CNF7, and CNF9 films, depicting the effect of increasing CNF concentration on the crystalline structure.

3.10 Mechanical properties

Table 3 presents the mechanical properties of CNF0 and CNF reinforced nanocomposite films. The mechanical properties of the films are further illustrated in Fig. 7 (a, b). Incorporation of CNFs into the cellulose matrix significantly increased both tensile strength and tensile modulus, while reducing elongation at break, consistent with previous studies. For instance, Faisal *et al.*[51] reported a similar increase in mechanical properties due to CNF incorporation in amylose-based films. In another study by Amri *et al.*[71], the incorporation of CNF improved the mechanical performance of the Jatropha Oil-Based Waterborne Polyurethane Film, with 0.5% CNF presence leading to maximum enhancement in tensile strength and Young's modulus.

Table 3. WVTR, OTR, and mechanical properties of CNF0 and the developed ACNC films

View Article Online
DOI: 10.1039/D6FB00014B

Samples	WVTR ($g/m^2/day$)	OTR ($cm^3/m^2/day$)	Tensile Strength (MPa)	Elongation at Break (%)	Tensile Modulus (GPa)
CNF0	180.4±4.8^a	52.7±2.2^a	45.3 ± 2.1^e	12.3 ± 1.2^a	0.68 ± 0.08^e
CNF3	129.8 ±5.2^b	43.8±2.4^b	61.8 ± 2.0^d	10.6 ± 1.0^a	1.75 ± 0.14^d
CNF5	85.3 ±4.1^c	24..7±1.7^c	73.1 ± 2.3^c	8.5 ± 0.9^b	2.43 ± 0.18^c
CNF7	44.7±3.0^e	5.6± 0.8^e	83.9 ± 1.5^a	7.8 ± 1.1^b	2.85 ± 0.15^b
CNF9	52.4 ±3.2^d	8.8± 0.1^d	80.4 ± 1.2^b	5.4 ± 0.6^c	3.12 ± 0.13^a

The values are given as the mean of three replicates ± SD (n=3). Mean values with different superscript letters in the same column are significantly different ($p \leq 0.05$).

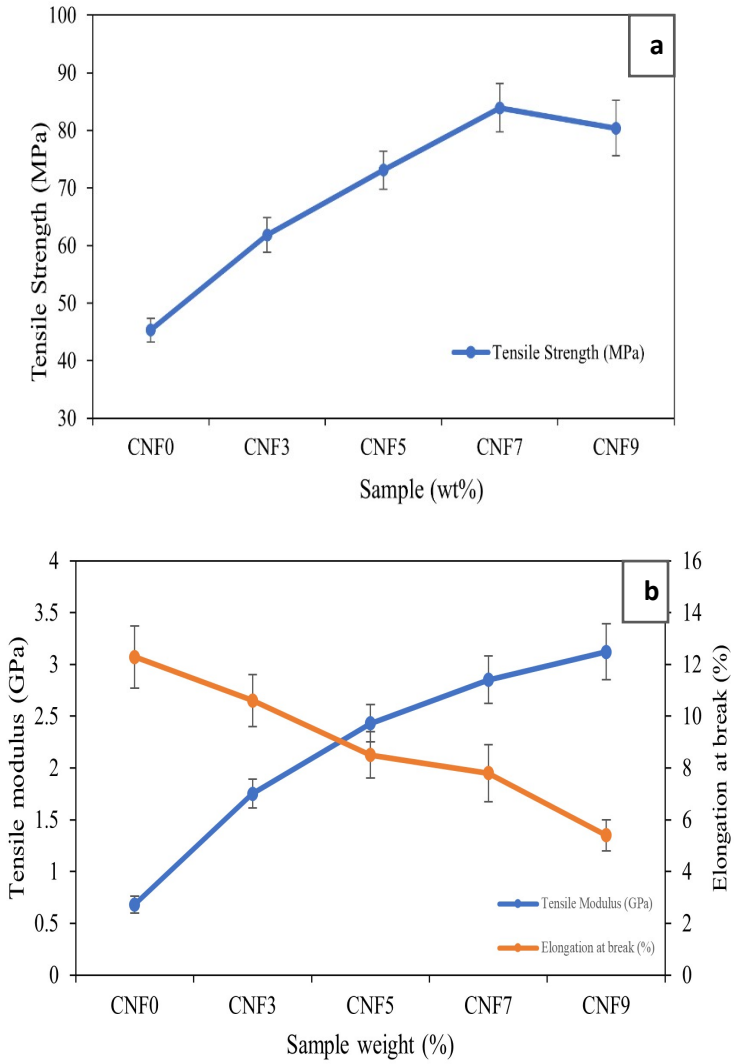

Fig. 7. (a) Tensile strength, and (b) Tensile modulus and elongation at break of CNF0 and the developed ACNC films, showing that increasing CNF concentrations led to higher tensile strength and tensile modulus, while elongation at break was decreased.

As per the data given in Table 3, the tensile strength increased from 45.3 ± 2.1 MPa for CNF0 to 83.9 ± 1.5 MPa for CNF7, which represented a statistically significant enhancement ($p \leq 0.05$). Similar enhancements have been reported in previous studies by Kesari *et al.*[58]; González

et al. [72], and Bian *et al.*[15]. It was attributed to strong interfacial interactions between the nanofibrils and the cellulose matrix, facilitated by their similar chemical composition, which effectively reinforced the film structure. [73]

As illustrated in the Fig. 9 (b), the reinforcing effect of CNFs arises from the formation of the entangled fibrous network within the cellulose matrix due to strong hydrogen bonding. As CNF concentration increases, these hydrogen-bonding interactions were enhanced, enabling an efficient stress transfer from the matrix to the nanofibers, thereby improving the tensile strength of the films.[74, 75] Shahi *et al.*[6] reported that improvement in tensile properties was due to the nanosize of CNF and homogenous dispersion, resulting in a compact and interconnected network in the matrix. This observation aligns with the present study, where CNF7 was found to be tougher than the CNF0 film. However, further increase in CNF concentration above 7 % led to a significant decrease in tensile strength, which could be the result of agglomeration (FE-SEM image Fig. 4e) and poor dispersion of CNF in the cellulose matrix.[50, 68]

The tensile modulus of CNF0 was measured to be 0.68±0.08 GPa (Table 3), and the incorporation of CNFs significantly increased it to 3.12±0.13 GPa in CNF9. The tensile modulus of the films was also affected by film density and moisture content (measured at 23 °C/50 % RH). With the increase in CNF content from CNF3 to CNF7, film density and modulus significantly increased, indicating that efficient nanofiber network formation within the matrix was established, which led to better support for the transfer of stress. The lower moisture content contributed to the higher stiffness of the films by reducing the mobility of the fibrils. However, in CNF9, density slightly decreased while moisture content increased because of fibril agglomeration that led to the formation of dense local bundles, and at the same time generated microvoids that promoted water absorption. Despite the higher moisture content in CNF9, tensile modulus remained high, as the stiff agglomerated fiber clusters dominated the mechanical response.

However, the elongation at break decreased with the nanofiber addition, with the most pronounced reduction observed in CNF9. At higher CNF concentrations, the increased fiber density likely reached a saturation point, restricting polymer chain mobility. A similar reduction in elongation at break with increasing CNF content was also observed by Wang *et al.*[76,] who isolated CNF from jute fibers for reinforcement in PVA film and attributed the decrease to the formation of a rigid network and increased stiffness that restricts chain mobility, thereby lowering film flexibility.[77] These results demonstrated that the incorporation of CNFs into cellulose nanocomposite films effectively improved their tensile strength and modulus; however, maintaining an optimal concentration is essential to prevent aggregation and resulting loss of flexibility.

3.11 Water Vapor Transmission Rate

Water vapor transmission rate (WVTR) is one of the most fundamental indicators of the barrier characteristics of packaging films, with lower values indicating greater water vapor resistance, which directly influences the texture, quality, and shelf life of food products.[78] Excess moisture in the films promotes microbial growth and accelerated food spoilage. The challenges, particularly concerning insufficient moisture barrier, significantly limit the usage of presently accessible biodegradable polymers in food packaging.[79] Incorporation of CNFs into the polymer matrix reduces WVTR[10, 80], likely by creating a physical barrier that hinders water vapor diffusion along the polymer–nanofiber interface. As shown in Fig. 8 (a), CNF0 exhibited a WVTR of 180.4 ± 4.8 g/m²/day, which decreased significantly to 44.7 ± 3.0 g/m²/day in CNF7, representing a 75.2% reduction. The WVTR values were observed to be significantly

different for all the films, indicating that the incorporation of CNFs progressively improved the water vapor barrier properties of films. The results are consistent with the findings of Rincon *et al.*[81] where CNFs were obtained from horticultural residues (mixture of bell pepper, tomato, and eggplant) and vine shoots, and reinforced in CMC films, which resulted in a 20-30% reduction in WVP compared to a neat CMC film. Guzman-Puyol *et al.*[11] reported approximately a 40% reduction in WVP for ACNC films containing 30% CNF, prepared using a solvent system comprising a mixture of Trifluoroacetic Acid and Trifluoroacetic Anhydride. Zhang *et al.*[82] reported that CNFs addition to polyhydroxybutyrate (PHB) films resulted in a 47.0% reduction in WVTR, decreasing from 298.7 to 140.4 g/(m^2 ·h). Lu *et al.*[83] reported that the WVTR of commercial polyethylene films ranges from 0.1 to 40 g/m^2/day, and the lowest value observed in the present study was comparable to this range of commercial packaging films. The enhanced moisture barrier is attributed to CNF-induced densification of the cellulose matrix, which restricts water vapor passage. High surface, dense network formation, and interfacial adhesion collectively and significantly enhanced the efficiency of the film by increasing the tortuosity of the diffusion path when positioned perpendicular to the direction of diffusion[79, 84, 85], as illustrated in Fig. 9 (b). Optimal CNF loading also minimizes polymer swelling and promotes the formation of an extensive hydrogen-bonded network, further strengthening structural integrity and interfacial interactions. [48, 86] Furthermore, CNFs incorporation resulted in a reduction of the moisture content of ACNC films (Table 2), which likely contributed to improved water vapor barrier properties. Since cellulose is hydrophilic and sensitive to moisture, water absorption triggers polymer swelling and plasticization, which leads to increased polymer chain mobility and remarkably reduced water vapor barrier properties of the film.[87,88]

The incorporation of nanofillers reduces the moisture content by reducing the free volume available in the matrix.[89,90] Similarly, Faisal *et al.*[51] reported a decrease in moisture content and WVTR due to the addition of CNF in amylose films. In the present investigation, moisture content, film density, and porosity have also been found to be related to WVTR, as higher levels of CNF reduced density, decreased porosity, and resulted in decreased WVTR. A positive correlation between CNF-induced variation in porosity and reduction in water vapor barrier properties has also been observed by Wei *et al.*[91] and Cainglet *et al.* [92].

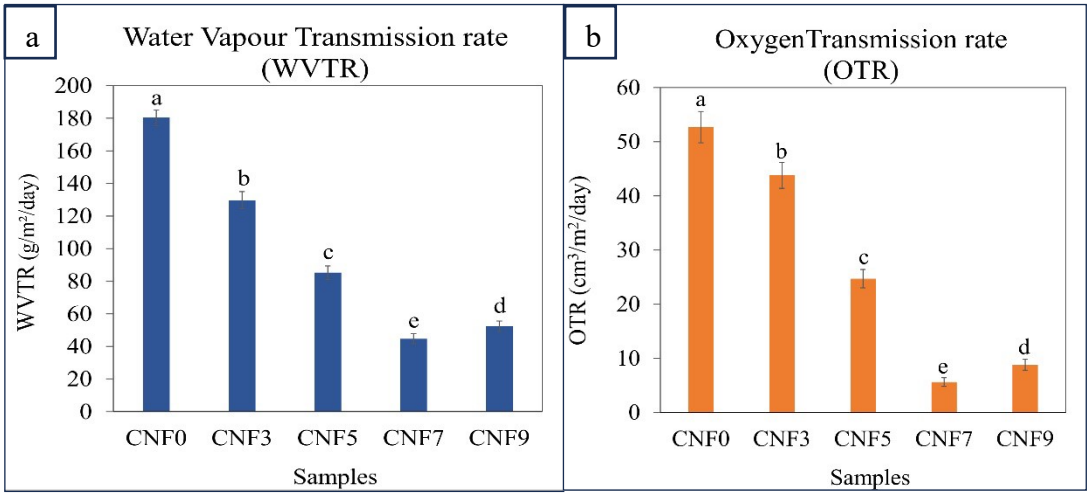

Fig. 8. (a) WVTR and (b) OTR of CNF0 and the developed ACNC films, showing a significant and progressive decrease with increasing CNFs concentration up to CNF7 (7%). Different

letters above the bars indicate statistically significant differences ($p \leq 0.05$) among the treatments.

View Article Online
DOI: 10.1039/D6FB00014B

3.12 Oxygen Transmission Rate

Oxygen is a critical extrinsic factor in food preservation, as its presence can promote oxidative degradation, microbial growth, rancidity, and browning, thereby compromising food quality. [93, 94] Like WVTR, oxygen transmission rate (OTR) is also crucial for assessing film barrier properties, which help extend shelf life, prevent spoilage, and preserve food quality.[10,95,96] The improvement in the oxygen barrier properties of the composite film due to the presence of CNF is significantly supported by previous studies.[51,97,98,99] Fig. 8 (b) displays the OTR as a function of CNF content, where a significant decrease was observed from CNF0 to CNF7 with increasing CNF loading. As shown in Table 3, the highest value of OTR observed in this study was 52.7±2.2 cm^3/m^2/day in CNF0, while CNF7 possessed the lowest OTR value of 5.6±0.8 cm^3/m^2/day, showing a reduction of OTR by ~ 89.3 %. Considering the OTR value for food packaging, which should typically be below 20 ml/m^2/day [100], the lowest OTR of CNF7 was a good indication of its oxygen barrier property. As illustrated in Fig 9 (b), this decreased OTR in CNF7 could be the result of tortuous path for diffusion of oxygen molecules due to CNF-induced nucleation, and recrystallization. In contrast, the absence of CNF in CNF0 resulted in a relatively lesser obstruction in the diffusion pathway, which led to higher OTR values (Fig 9a).

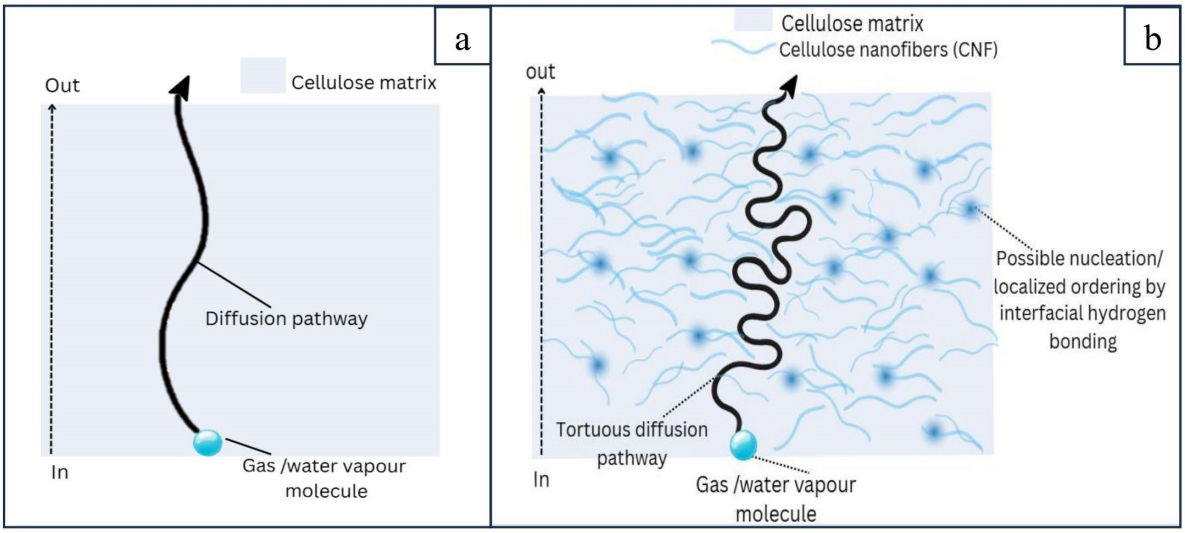

Fig. 9. Schematic representation of diffusion pathways in (a) CNF0 and (b) CNF7, showing CNF-induced nucleation, recrystallization, and increased tortuosity, leading to reduced WVTR and OTR of ACNC films.

Similar improvement in oxygen barrier property due to the incorporation of CNF has been validated in a previous study by Faisal *et al.*[51,] who compared the reinforcing effect of CNC and CNF in amylose film and found that the presence of 3% nanofibrils resulted in improved gas barrier properties compared to the composite prepared with 3% CNC. Nguyen *et al.*[77] developed composite films by adding boron nitride nanosheets to the CNF film for the meat and cheese packaging, and observed that OTR values were reduced to 4.7 cc/m^2/day in the film containing 5% nanosheets, which was comparable with the OTR for CNF7 obtained in the

present study. It was worth noting that the OTR improvement aligned well with the high tensile strength as the reinforcement effect of CNF, which promoted the creation of a strong hydrogen-bonded cohesive network due to high surface area and nanoscale size.[101] Interestingly, a positive correlation between OTR, porosity, density, and moisture content of the films was evident in this study. The incorporation of CNFs into the matrix led to a reduction in the porous structure of the films, with CNF7 exhibiting the lowest porosity and correspondingly reduced OTR. The nanosized fibers could have filled the voids within the polymer matrix, decreased free volume, enhanced nanofiber-polymer contact, and facilitated effective stress transfer at the interface. These observations were consistent with the measured density values, indicating that the dense structure formed in the ACNC films likely extended the diffusion path for oxygen molecules perpendicular to the film orientation.[9, 102,] A similar trend was also observed in the moisture content values, which demonstrated a clear dependence of oxygen barrier performance on moisture content, as the presence of moisture can act as a plasticiser and disturb hydrogen bonding. This can lead to a lowering of cohesive energy with an increase in porosity[103], resulting in passage through, which molecules that can permeate.[104] However, the presence of CNF promotes the formation of a stronger hydrogen-bonded structure, and compact fiber alignment tends to slow down the transmission[105] and limit polymer chain mobility. The improvement in structural properties and barrier performance correlated well with the CNF concentration, with maximum improvement observed in CNF7. As the CNF concentration increased further, the agglomeration of CNF affected the functionality of the film. This is due to the intrinsic tendency of CNF to agglomerate as a result of strong intermolecular hydrogen bonding and van der Waals interactions, which leads to uneven dispersion within the matrix, affecting film properties.[48] Additionally, Crystallinity also plays a significant role in restricting oxygen transport through the nanocomposite film. CNF with high crystallinity may act as a nucleating agent and interact strongly with the polymer matrix, promoting H-bonding and intercrosslinking, which can improve gas barrier properties.[106] A similar effect was observed in the present study, as the sample with higher crystallinity had enhanced oxygen barrier performance. Belbekhouche *et al.*[107] attributed lower oxygen barrier properties in cellulose nanofiber (CNF) compared to cellulose nanocrystal (CNC) films to their higher density, and enlargement of the fibrous network. Nair *et al.* [108] observed that the higher crystallinity and morphology of nanofibers in the film led to an intricate structure due to fibrous entanglement, forming a complex structure having low porosity and increased tortuosity, which resulted in reduced OTR.

3.13 Optical transmittance

Optical transmittance is a functional criterion for assessing the compatibility and miscibility of composite components. High transparency is particularly desirable in food packaging applications as it enhances visual appeal and consumer acceptance. Table 4 presents the optical transmittance values at a wavelength of 800 nm for all the film samples. The CNF0 exhibited a high transmittance of 90.05±0.21 %, demonstrating excellent transparency. The CNF3 and CNF5 showed slightly reduced transmittance values of 88.13±0.38 % and 86.74±0.29 %, respectively, while CNF9 decreased further to 79.19±0.31%. The results obtained are consistent with the findings of Zhao *et al.*[36] where a decrease in optical transmittance was observed with increasing CNF content (5% to 20%) in the ACNC films, with the lowest

transmittance being 75.97% in the film containing 20% CNF. Similarly, Wang *et al*.[76] reported that the optical transmittance of PVA film was slightly decreased due to CNF incorporation, with PVA film containing 2% CNF exhibiting the lowest optical transmittance of 77.55%. This reduction in transmittance most likely occurred due to the elevated light scattering caused by the presence of CNF, as well as a slight difference in refractive index[109]between CNF and the matrix and potential micro-aggregation within the film. The observed behaviour demonstrated that, despite the slight reduction with CNF presence, the transmittance remained relatively favourable (86.111 ±0.35%, %) in CNF7, indicating that the film retained good optical clarity, which is desirable for food packaging.

The color of films for food packaging is an important quality parameter. It was observed that the optical properties of the ACNCs were influenced significantly by the increasing CNF content (Table 4). The value of lightness (L) decreased significantly from 95.37 ± 0.29 in the control (CNF0) to 91.28 ± 0.33 in CNF9, whereas the value of chroma increased significantly from 1.14 to 2.36. The observed decrease of the lightness (L^*) and increase of chroma (C^*) as a function of the CNF content could most likely be due to the increase of light scattering and opacity caused by the nanofibril network. The significant decrease in hue angle (H^o) from 105.5 ° to 94.1 ° indicated that incorporation of CNF affected saturation rather than the overall color tone. The overall color difference (ΔE_{ab}) compared to the control increased from 0 to 4.28, which demonstrated the perceptible color variations with an increase in CNF content. This finding aligns with the results reported by Fan et al[210], where a variation was observed in the L^* and b^* values between hyaluronic acid composite film and hyaluronic acid-curcumin-cellulose nanofibre composite film, with the difference being influenced by the CNF addition. Similarly, Mohammadi et al[211] observed an increased ΔE value of the nanocomposites when chitosan nanofibers were included in a carboxymethyl cellulose matrix.

Table 4. Transmittance (Tr), Color parameters (L^*, a^*, b^*), chroma (C^*), hue angle (H°) and total color difference (ΔE_{ab}) of film samples

Samples	Tr (%)	L^*	a^*	b^*	C^*	H°	ΔE_{ab}
CNF0	90.05 ± 0.21^a	95.37 ± 0.29^a	-0.30 ± 0.02^c	1.1 ± 0.12^a	1.14^a	105.5^a	0
CNF3	88.13 ± 0.38^b	94.30 ± 0.32^b	-0.27 ± 0.04^b	1.31 ± 0.14^a	1.34^a	101.7^a	1.09
CNF5	86.74 ± 0.29^c	93.77 ± 0.20^c	-0.23 ± 0.04^a	1.75 ± 0.15^b	1.77^b	97.6^b	1.73
CNF7	86.11 ± 0.35^d	93.38 ± 0.28^c	-0.21 ± 0.03^a	2.03 ± 0.13^c	2.04^c	94.1^b	2.11
CNF9	79.19 ± 0.31^e	91.28 ± 0.33^d	-0.17 ± 0.05^a	2.35 ± 0.18^d	2.36^d	93.9^b	4.28

Mean values with different superscript letters in the same column are significantly different ($p \leq 0.05$).

3.14 Thermogravimetric Analysis

Fig. 10 (A, B) depicts the TGA and DTG curves of CNF0 and ACNC films, providing insight into their thermal stability and degradation behaviour. Thermal degradation of all films occurred in three distinct degradation stages. The initial stage, between 33 °C and 201 °C, was attributed to the evaporation of physically adsorbed moisture.[112] The main decomposition stage,

View Article Online
DOI: 10.1039/D6FB00014B

observed from 206 ºC to 462 ºC, corresponded to pyrolysis of cellulose during which glycosidic linkages and carboxylic groups attached to the glucose units were cleaved.[68,101] The peak degradation temperature (Td) varied among the ACNC films, with CNF7 exhibiting the highest (335.40 ºC), while CNF0 had the lowest (315.68 ºC). This shift is attributed to CNF reinforcement, consistent with previous studies: Kesari *et al.*[58] observed an increase from 311.58 °C for neat thermoplastic starch film to 319 °C with 5% CNF, and Bian *et al.*[15] reported a rise from 290 °C in wheat straw cellulose film to 327 °C with 3% CNF. Gan *et al.*[113] noted that CNF reinforcement and enhanced interfacial adhesion restrict polymer chain mobility, raising the energy barrier for thermal degradation.[50] TGA curves also showed that nanocomposite films had lower weight loss rates than CNF0 films, indicating improved heat stability. The third degradation stage occurs between 423.33 ºC to 597.61ºC °C, which leads to the thermal decomposition of charred residue into gaseous byproducts.[114] The above findings suggested that the presence of CNF as a nanofiller reinforcement in the nanocomposite made the film more resistant to thermal stress.[76]

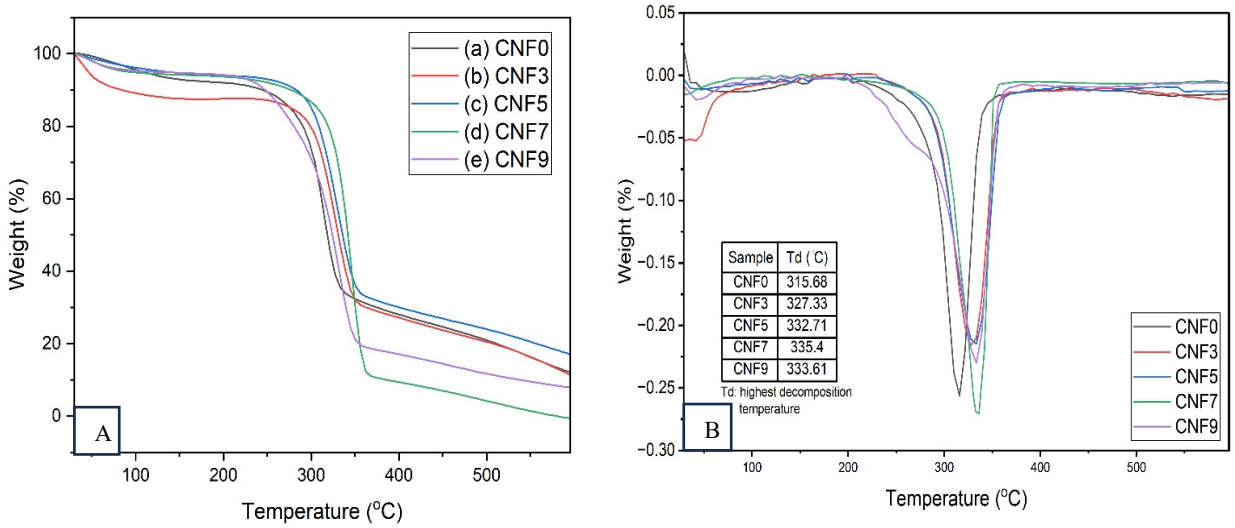

Fig. 10. The (A) TGA, and (B) DTG thermograms of the developed ACNC films. The insert in the DTG thermogram shows the degradation temperatures (Td) of ACNCs, with CNF7 exhibiting the maximum value.

3.15 Biodegradability

The biodegradation behavior of CNF0 and CNF7 was assessed by monitoring weight loss over time under enzymatic conditions. The biodegradability test setup, showing film samples incubated in reagent bottles inside a controlled B.O.D. incubator, is displayed in Fig. 11. Cellulase hydrolyzed the β-1,4 glycosidic bonds of cellulose, leading to the release of soluble sugars that diffused into the medium. Consequently, the film samples became solubilized or degraded into fragments, resulting in a gradual loss of weight over time. As shown in Fig. 12, the incorporation of CNFs affected the degradation rate of all cellulose nanocomposite films (CNF7) in the enzymatic solution. CNF0 exhibited a higher biodegradation rate compared to CNF7, likely due to the dense hydrogen-bonded network formed between the cellulose matrix and CNFs, which slowed enzymatic breakdown.

View Article Online
DOI: 10.1039/D6FB00014B

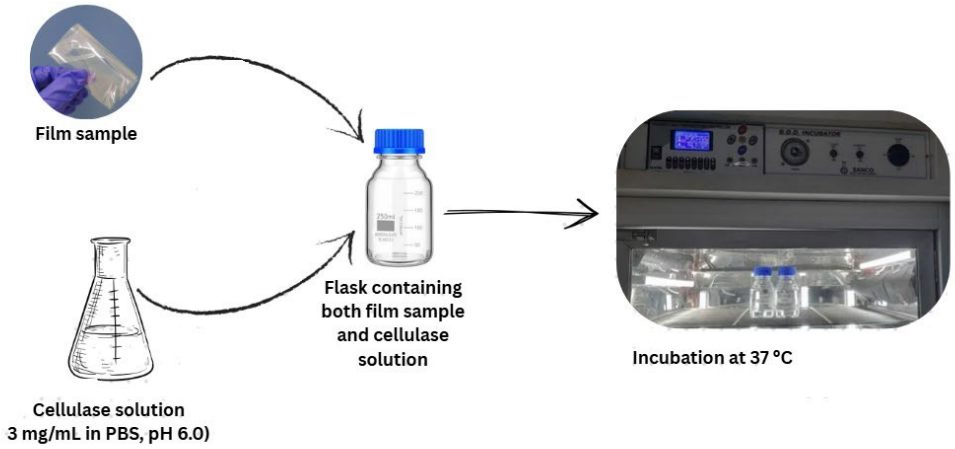

Fig. 11. Experimental setup for the enzymatic degradation of films. Film samples were placed in the cellulase solution and incubated at 37 °C. The enzymatic degradation of the films was monitored with time.

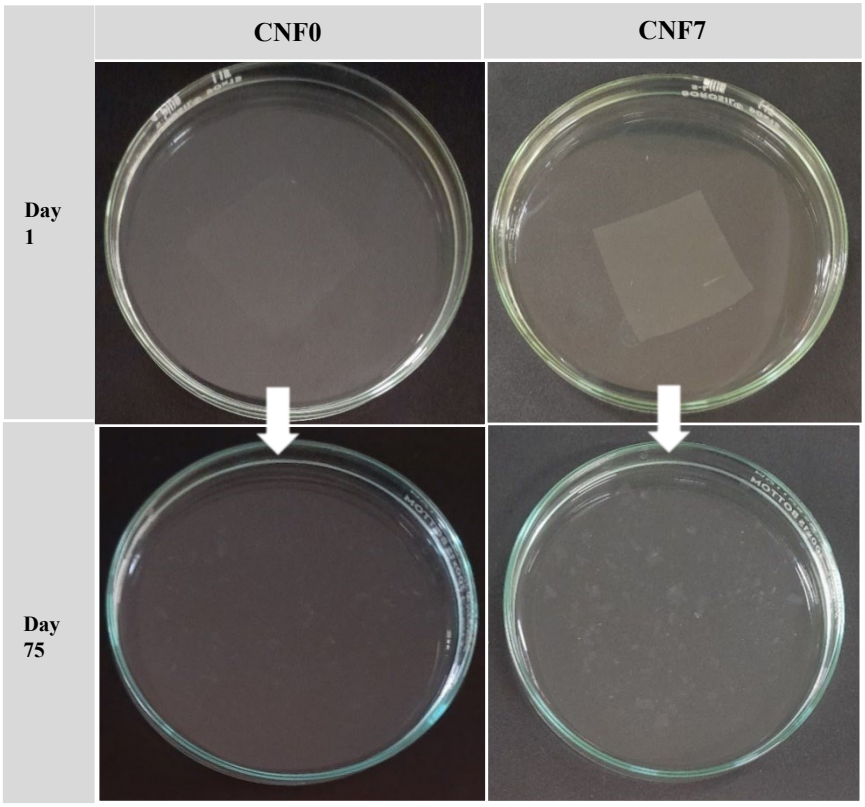

Fig. 12. Biodegradation of CNF0 and CNF7 films in cellulase enzyme solution. A higher number of fragments was observed in the CNF0 petriplate compared to the CNF7, which indicated relatively slightly faster disintegration during enzymatic degradation in CNF0

Table 5. Biodegradable behaviour (% weight loss) of CNF0 and CNF7 films

View Article Online
DOI: 10.1039/D6FB00014B

Sample	Incubation Time (Days)				
	15	30	45	60	75
CNF0	17.3 ± 1.1^{eA}	36.3 ± 1.4^{dA}	56.8 ± 2.4^{cA}	72.2 ± 2.1^{bA}	94.4 ± 1.5^{aA}
CNF7	14.7 ± 0.9^{eB}	32.6 ± 1.2^{dB}	49.8 ± 0.9^{cB}	69.5 ± 2.2^{bB}	89.4 ± 2.2^{aB}

Values are represented as mean ± SD (n=3). Means values with different small superscripts letters within the row and capital superscripts letters within the column of a parameter are significantly different ($p\leq0.05$).

As shown in Table 5, CNF0 exhibited a significantly higher biodegradation rate than CNF7, and this trend persisted throughout the incubation period. After 75 days of incubation, there was 94.4% biodegradation of CNF0, while it was 89.4% for CNF7. The slower enzymatic degradation of CNF7 could likely be due to variation in film morphology, as the addition of CNF may have resulted in a strong hydrogen-bonded network between the cellulose matrix and CNFs due to the homogenous dispersion of CNF. Additionally, the higher crystallinity of CNFs, as reported in our earlier study [22] may have also contributed to slightly reduced biodegradability of the ACNC films. Since enzymatic hydrolysis generally initiates at the amorphous regions, followed by gradual degradation of the crystalline regions[115], the reinforcement of CNF reduced the proportion of amorphous cellulose available for enzymatic degradation, and thus slowed the degradation rate. A similar observation was reported by Louis et al.[116], where nanocellulose-reinforced starch films exhibited a slower degradation rate than pure starch films under the soil burial method.

4. Conclusion

The present study successfully demonstrated the development of all-cellulose nanocomposite films derived from rice straw and reinforced with cellulose nanofibers (CNFs) using a LiCl/DMAc solvent system. The ACNC films were prepared with process parameters optimized to prevent dimensional shrinkage. The study provided a comprehensive evaluation of the films' structural, mechanical, optical, thermal, barrier, and biodegradability properties, highlighting their relevance to sustainable food packaging applications. The study also offered a systematic and comprehensive understanding of the structure-property relationship that controlled the performance of the films. The film containing 7% CNFs showed the highest tensile strength and tensile modulus, while maintaining adequate extensibility. The low OTR and WVTR of CNF7 were a good indication of its barrier properties, which were comparable to the range of other commercial packaging films. The developed ACNC film possessed lower moisture content and sufficiently good biodegradability. Overall, the ACNC film (CNF7) could be considered as a promising biodegradable and eco-friendly alternative to commercial non-biodegradable polyethylene films or the other packaging materials. The use of abundantly available underutilised rice straw for the development of the film meets the single feedstock circular approach. The ability to achieve desirable film properties at low CNF loading of 7% highlights the cost-effectiveness and sustainability of the developed system for food packaging applications.

Further investigations are required to evaluate the heat-sealability and self-bonding characteristics of ACNC films to establish their commercial viability. However, for large-scale applications, the LiCl/DMAc solvent system may be replaced with more environmentally friendly and scalable alternatives, such as NaOH/urea/water or deep eutectic solvents, to

enhance sustainability, safety, and regulatory compliance for food packaging applications. In addition, efficient recovery and recycling of solvents after film production will be critical for promoting environmental compatibility and industrial scalability. Future research should also investigate the performance of the developed ACNC films across a wider range of food systems under diverse environmental and storage conditions.

Acknowledgements: The authors gratefully acknowledge the Analytical Chemistry Lab, Sharda University, Greater Noida, Central Instrumentation Laboratory (CIL), Guru Jambheshwar University of Science & Technology, Hisar, Haryana, the University Science Instrumentation Centre (USIC), University of Delhi, and the Central Research Facility (CRF), IIT Delhi, New Delhi, India, for the instrumentation facilities that greatly facilitated our research.

Author contribution: Sadhana Jadaun: Investigation, data curation, and interpretation, writing original draft. Saleem Siddiqui: conceptualization, supervision, data interpretation, manuscript reviewing. Sneh Punia Bangar: validation, manuscript reviewing, and editing.

Funding: This research received no external funding.

References

1. B. Nath, M. M. Ahmmed, S. Paul, M. D. Huda, M. A. Hossain and S. Islam, Unlocking the potential of rice straw: Sustainable utilization strategies for Bangladesh, *Circular Economy*, 2025, **4**, 100126, DOI: https://doi.org/10.1016/j.cec.2025.100126
2. P. Roy, S. Bhattacharyya, M. Kaur, K. M. Sharma, M. Barman, A. G. Choudhury and P. Bhowmick, Comprehensive scenario analysis of straw management in Punjab and West Bengal, in *Technological Advancement and Use of Artificial Intelligence in Climate Smart Agriculture*, International Books & Periodical Supply Service, 2023, pp. 187–199
3. D. S. Parihar, M. K. Narang, B. Dogra, A. Prakash and A. Mahadik, Rice residue burning in Northern India: an assessment of environmental concerns and potential solutions – a review, *Environ. Res. Commun.*, 2023, **5**, 062001, DOI: https://doi.org/10.1088/2515-7620/acb6d4.
4. A. K. Sakhiya, P. Kaushal and V. K. Vijay, Process optimization of rice straw-derived activated biochar and biosorption of heavy metals from drinking water in rural areas, *Appl. Surf. Sci. Adv.*, 2023, **18**, 100481, DOI: https://doi.org/10.1016/j.apsadv.2023.100481.
5. Y. Singh, S. Sharma, U. Kumar, P. Sihag, P. Balyan, K. P. Singh and O. P. Dhankher, Strategies for economic utilization of rice straw residues into value-added by-products and prevention of environmental pollution, *Sci. Total Environ.*, 2024, **906**, 167714, DOI: https://doi.org/10.1016/j.scitotenv.2023.167714.
6. N. Shahi, B. Min, B. Sapkota and V. K. Rangari, Eco-friendly cellulose nanofiber extraction from sugarcane bagasse and film fabrication, *Sustainability*, 2020, **12**, 6015, DOI: https://doi.org/10.3390/su12156015.
7. S. Mandin, S. Moreau, M. Talantikite, B. Novalès, J.-E. Maigret, B. Cathala and C. Moreau, Cellulose nanofibrils/xyloglucan bio-based aerogels with shape recovery, *Gels*, 2021, **7**, 5, DOI: https://doi.org/10.3390/gels7010005.

8. B. N. Altay, B. Aksoy, J. Atkinson, C. L. Lewis, C. Diaz-Acosta and R. Francis, Flow dynamics of agricultural waste nanofibers: shear, temperature, and oscillatory insights, *Cellulose*, 2025, **32**, 3077–3094, DOI: https://doi.org/10.1007/s10570-025-06444-8.
9. T. D. Moshood, G. Nawanir, F. Mahmud, F. Mohamad, M. H. Ahmad and A. AbdulGhani, Sustainability of biodegradable plastics: new problem or solution to solve the global plastic pollution?, *Curr. Res. Green Sustain. Chem.*, 2022, **5**, 100273, DOI: https://doi.org/10.1016/j.crgsc.2022.100273.
10. L. Jing, T. Shi, Y. Chang, X. Meng, S. He, H. Xu, S. Yang and J. Liu, Cellulose-based materials in environmental protection: a scientometric and visual analysis review, *Sci. Total Environ.*, 2024, **929**, 172576, DOI: https://doi.org/10.1016/j.scitotenv.2024.172576.
11. S. Guzmán-Puyol, L. Ceseracciu, G. Tedeschi, S. Marras, A. Scarpellini, J. J. Benítez, A. Athanassiou and J. A. Heredia-Guerrero, Transparent and robust all-cellulose nanocomposite packaging materials prepared in a mixture of trifluoroacetic acid and trifluoroacetic anhydride, *Nanomaterials*, 2019, **9**, 368, DOI: https://doi.org/10.3390/nano9030368.
12. E. S. Nascimento, M. O. Barros, M. A. Cerqueira, H. L. Lima, M. D. F. Borges, L. M. Pastrana, F. M. Gama, M. F. Rosa, H. M. C. Azeredo and C. Gonçalves, All-cellulose nanocomposite films based on bacterial cellulose nanofibrils and nanocrystals, *Food Packag. Shelf Life*, 2021, **29**, 100715, DOI: https://doi.org/10.1016/j.fpsl.2021.100715.
13. C. Rader, L. Grillo and C. Weder, Water and oxygen barrier properties of all-cellulose nanocomposites, *Biomacromolecules*, 2024, **25**, 1906–1915, DOI: https://doi.org/10.1021/acs.biomac.3c01337.
14. Q. Yang, T. Saito, L. A. Berglund and A. Isogai, Cellulose nanofibrils improve the properties of all-cellulose composites by the nano-reinforcement mechanism and nanofibril-induced crystallization, *Nanoscale*, 2015, **7**, 17957–17963, DOI: https://doi.org/10.1039/C5NR05511C.
15. H. Bian, Y. Yang, P. Tu and J. Y. Chen, Value-added utilization of wheat straw: from cellulose and cellulose nanofiber to all-cellulose nanocomposite film, *Membranes*, 2022, **12**, 475, DOI: https://doi.org/10.3390/membranes12050475.
16. M. Ghaderi, M. Mousavi, H. Yousefi and M. Labbafi, All-cellulose nanocomposite film made from bagasse cellulose nanofibers for food packaging application, *Carbohydr. Polym.*, 2014, **104**, 59–65, DOI: https://doi.org/10.1016/j.carbpol.2014.01.013.
17. M. Z. E. Sinaga, S. Gea, N. Panindia and Y. A. Sihombing, The preparation of all-cellulose nanocomposite film from isolated cellulose of corncobs as food packaging, *Orient. J. Chem.*, 2018, **34**, 1, DOI: https://doi.org/10.13005/ojc/340166.
18. M. Fazeli, M. Keley and E. Biazar, Preparation and characterization of starch-based composite films reinforced by cellulose nanofibers, *Int. J. Biol. Macromol.*, 2018, **116**, 272–280, DOI:https://doi.org/10.1016/j.ijbiomac.2018.04.186
19. J. C. Alcántara, I. González, M. M. Pareta and F. Vilaseca, Biocomposites from rice straw nanofibers: morphology, thermal and mechanical properties, *Materials*, 2020, **13**, 2138, DOI: https://doi.org/10.3390/ma13092138.
20. X. Zhong, Y. Pan, Z. Feng, Z.-B. Shao, J. Qiu and L. Zhu, Rice straw-based cellulose nanofiber reinforcing polyvinyl alcohol antibacterial film through electrospinning, *Compos. Commun.*, 2024, **49**, 101972, DOI: https://doi.org/10.1016/j.coco.2024.101972.
21. M. Islam, A. S. K. Sinha and K. Prasad, Rice straw biomass-based modified cellulose nanofibers (CNFs): reinforcement in polylactic acid (PLA) bio nanocomposite films, *Biomass Convers. Biorefin.*, 2026, **16**, 2, DOI: https://doi.org/10.1007/s13399-025-06962-2.

22. S. Jadaun, N. Upadhyay and S. Siddiqui, Isolation and characterization of cellulose nanofibers from rice straw using ultrasonication-assisted extraction technique coupled with high shear dispersion, *Biomass Convers. Biorefin.*, 2025, **15(16)**, 23629–23645, DOI: https://doi.org/10.1007/s13399-025-06740-0.
23. P. J. V. Soest and R. H. Wine, Use of detergents in the analysis of fibrous feeds. IV. determination of plant cell-wall constituents, *J. AOAC Int.*, 1967, **50**, 50–55, DOI: https://doi. org/10.1093/jaoac/50.1.50
24. K. Pradhan and S. K. Bhatia, Modification, standardization and evolving chemical and biological techniques for nutritive evaluation of forage, Technical Bulletin, Department of Animal Nutrition, HAU, Hisar, 1986.
25. N. Kadivar, H. Tavanai and A. Allafchian, Fabrication of cellulose nanoparticles through electrospraying, *IET Nanobiotechnol.*, 2018, **12**, 807–813, DOI: https://doi.org/10.1049/iet-nbt.2018.0044.
26. S. Maraghechi, A.-L. Dupont, R. Cardinaels, S. Paris-Lacombe, J. P. M. Hoefnagels, A. S. J. Suiker and E. Bosco, Assessing rheometry for measuring the viscosity-average degree of polymerisation of cellulose in paper degradation studies, *Herit. Sci.*, 2023, **11**, 15, DOI: https://doi.org/10.1186/s40494-022-00855-7.
27. X. Hao, W. Shen, Z. Chen, J. Zhu, L. Feng, Z. Wu, P. Wang, X. Zeng and T. Wu, Self-assembled nanostructured cellulose prepared by a dissolution and regeneration process using phosphoric acid as a solvent, *Carbohydr. Polym.*, 2015, **123**, 297–304, DOI: https://doi.org/10.1016/j.carbpol.2015.01.055.
28. C. L. McCormick, P. A. Callais and B. H. Hutchinson, Solution studies of cellulose in lithium chloride and N,N-dimethylacetamide, *Macromolecules*, 1985, **18**, 2394–2401, DOI: https://doi.org/10.1021/ma00154a010.
29. L. Segal, J. J. Creely, A. E. Martin and C. M. Conrad, An empirical method for estimating the degree of crystallinity of native cellulose using the X-ray diffractometer, *Text. Res. J.*, 1959, **29**, 786–794, DOI: https://doi.org/10.1177/004051755902901003.
30. Y. Zahedi, B. Fathi-Achachlouei and A. R. Yousefi, Physical and mechanical properties of hybrid montmorillonite/zinc oxide reinforced carboxymethyl cellulose nanocomposites, *Int. J. Biol. Macromol.*, 2018, **108**, 863–873, DOI: https://doi.org/10.1016/j.ijbiomac.2017.10.185.
31. N. Yousefi, Y. Zahedi, A. Yousefi, G. Hosseinzadeh and M. Jekle, Development of carboxymethyl cellulose-based nanocomposite incorporated with ZnO nanoparticles synthesized by cress seed mucilage as green surfactant, *Int. J. Biol. Macromol.*, 2024, **265**, 130849, DOI: https://doi.org/10.1016/j.ijbiomac.2024.130849.
32. C. Liang, J. Zhang, G. Fu, Z. Jin, Q. Lu, X. Li and D. Yue, Effect of bonding on the structure and properties of nanocellulose films, *BioResources*, 2022, **17**, 6761–6774, DOI: https://doi.org/10.15376/biores.17.4.6761-6774.
33. X. Yang, F. Berthold and L. A. Berglund, High-density molded cellulose fibers and transparent biocomposites based on oriented holocellulose, *ACS Appl. Mater. Interfaces*, 2019, **11**, 10310–10319, DOI: https://doi.org/10.1021/acsami.8b22134.
34. A. G. Souza, R. R. Ferreira, L. C. Paula, S. K. Mitra and D. S. Rosa, Starch-based films enriched with nanocellulose-stabilized Pickering emulsions containing different essential oils for possible applications in food packaging, *Food Packag. Shelf Life*, 2021, **27**, 100615, DOI: https://doi.org/10.1016/j.fpsl.2020.100615.
35. W. G. Sganzerla, L. E. N. Castro, C. G. Da Rosa, A. D. R. Almeida, F. W. Maciel-Silva, P. R. G. Kempe, A. L. R. De Oliveira, T. Forster-Carneiro, F. C. Bertoldi, P. L. M. Barreto, A. P. D. L. Veeck and M. R. Nunes, Production of nanocomposite films functionalized with silver nanoparticles bioreduced with rosemary (*Rosmarinus officinalis* L.) essential oil, *J. Agric. Food Res.*, 2023, **11**, 100479, DOI: https://doi.org/10.1016/j.jafr.2022.100479.

36. J. Zhao, X. He, Y. Wang, W. Zhang, X. Zhang, X. Zhang, Y. Deng and C. Lu, Reinforcement of all-cellulose nanocomposite films using native cellulose nanofibrils, *Carbohydr. Polym.*, 2014, **104**, 143–150, DOI: https://doi.org/10.1016/j.carbpol.2014.01.007.
37. J.-K. Kim, B. Choi and J. Jin, Transparent, water-stable, cellulose nanofiber-based packaging film with a low oxygen permeability, *Carbohydr. Polym.*, 2020, **249**, 116823, DOI: https://doi.org/10.1016/j.carbpol.2020.116823.
38. C. Rovera, D. Carullo, T. Bellesia, D. Büyüktaş, M. Ghaani, E. Caneva and S. Farris, Extraction of high-quality grade cellulose and cellulose nanocrystals from different lignocellulosic agri-food wastes, *Front. Sustain. Food Syst.*, 2023, **6**, 1087867, DOI: https://doi.org/10.3389/fsufs.2022.1087867.
39. Q. Wang, J. Y. Zhu and J. M. Considine, Strong and optically transparent films prepared using cellulosic solid residue recovered from cellulose nanocrystals production waste stream, *ACS Appl. Mater. Interfaces*, 2013, **5**, 2527–2534, DOI: https://doi.org/10.1021/am302967m.
40. Y. Zhou, X. Zhang, J. Zhang, Y. Cheng, J. Wu, J. Yu and J. Zhang, Molecular weight characterization of cellulose using ionic liquids, *Polym. Test.*, 2021, **93**, 106985, DOI: https://doi.org/10.1016/j.polymertesting.2020.106985.
41. S. Acharya, S. Liyanage, P. Parajuli, S. S. Rumi, J. L. Shamshina and N. Abidi, Utilization of cellulose to its full potential: a review on cellulose dissolution, regeneration, and applications, *Polymers*, 2021, **13**, 4344, DOI: https://doi.org/10.3390/polym13244344.
42. J. Oberlerchner, T. Rosenau and A. Potthast, Overview of methods for the direct molar mass determination of cellulose, *Molecules*, 2015, **20**, 10313–10341, DOI: https://doi.org/10.3390/molecules200610313.
43. M. Dilamian and B. Noroozi, A combined homogenization-high intensity ultrasonication process for individualization of cellulose micro-nano fibers from rice straw, *Cellulose*, 2019, **26**, 5831–5849, DOI: https://doi.org/10.1007/s10570-019-02469-y.
44. B. Du, S. P. K. Jeepipalli and B. Xu, Critical review on alterations in physicochemical properties and molecular structure of natural polysaccharides upon ultrasonication, *Ultrason. Sonochem.*, 2022, **90**, 106170, DOI: https://doi.org/10.1016/j.ultsonch.2022.106170.
45. S. Zhang, S. Shan, H. Zhang, X. Gao, X. Tang and K. Chen, Antimicrobial cellulose hydrogels preparation with RIF loading from bamboo parenchyma cells: a green approach towards wound healing, *Int. J. Biol. Macromol.*, 2022, **203**, 1–9, DOI: https://doi.org/10.1016/j.ijbiomac.2022.01.046.
46. X. Liu, Z. Qin, Y. Ma, H. Liu and X. Wang, Cellulose-based films for food packaging applications: review of preparation, properties, and prospects, *J. Renew. Mater.*, 2023, **11**, 3203–3225, DOI: https://doi.org/10.32604/jrm.2023.027613.
47. R. Moreira, R. C. Rebelo, J. F. J. Coelho and A. C. Serra, Novel thermally regenerated flexible cellulose-based films, *Eur. J. Wood Prod.*, 2024, **82**, 1813–1826, DOI: https://doi.org/10.1007/s00107-024-02126-7.
48. S. A. Jose, N. Cowan, M. Davidson, G. Godina, I. Smith, J. Xin and P. L. Menezes, A comprehensive review on cellulose nanofibers, nanomaterials, and composites: manufacturing, properties, and applications, *Nanomaterials*, 2025, **15**, 356, DOI: https://doi.org/10.3390/nano15050356.
49. S. S. Shazleen, T. A. T. Yasim-Anuar, N. A. Ibrahim, M. A. Hassan and H. Ariffin, Functionality of cellulose nanofiber as bio-based nucleating agent and nano-reinforcement material to enhance crystallization and mechanical properties of

polylactic acid nanocomposite, *Polymers*, 2021, **13**, 389, DOI: https://doi.org/10.3390/polym13030389.

50. S. S. Nordi, E. E. M. Noor, C. K. Kok, N. M. Julkapli and M. F. Baig, Phase, chemical, thermal, and morphological analyses of thermoplastic polyurethane (TPU) nanocomposites reinforced with jute cellulose nanofibers (CNFs), *Polymers*, 2025, **17**, 899, DOI: https://doi.org/10.3390/polym17070899.
51. M. Faisal, M. Žmirić, N. Kim, S. Bruun, L. Mariniello, M. Famiglietti, H. Bordallo, J. Kirkensgaard, B. Jørgensen, P. Ulvskov, K. Hebelstrup and A. Blennow, A comparison of cellulose nanocrystals and nanofibers as reinforcements to amylose-based composite bioplastics, *Coatings*, 2023, **13**, 1573, DOI: https://doi.org/10.3390/coatings13091573.
52. R. Vârban, I. Crișan, D. Vârban, A. Ona, L. Olar, A. Stoie and R. Ștefan, Comparative FT-IR prospecting for cellulose in stems of some fiber plants: flax, velvet leaf, hemp and jute, *Appl. Sci.*, 2021, **11**, 8570, DOI: https://doi.org/10.3390/app11188570.
53. M. Sadeghi-Shapourabadi, S. Elkoun and M. Robert, Microwave-assisted chemical purification and ultrasonication for extraction of nano-fibrillated cellulose from potato peel waste, *Macromol*, 2023, **3**, 766–781, DOI: https://doi.org/10.3390/macromol3040044.
54. M. M. Rana and H. De La Hoz Siegler, Influence of ionic liquid (IL) treatment conditions in the regeneration of cellulose with different crystallinity, *J. Mater. Res.*, 2023, **38**, 328–336, DOI: https://doi.org/10.1557/s43578-022-00797-7.
55. R. Md Salim, J. Asik and M. S. Sarjadi, Chemical functional groups of extractives, cellulose and lignin extracted from native *Leucaena leucocephala* bark, *Wood Sci. Technol.*, 2021, **55**, 295–313, DOI: https://doi.org/10.1007/s00226-020-01258-2.
56. E. Aigaje, A. Riofrio and H. Baykara, Processing, properties, modifications, and environmental impact of nanocellulose/biopolymer composites: a review, *Polymers*, 2023, **15**, 1219, DOI: https://doi.org/10.3390/polym15051219.
57. B. Deepa, E. Abraham, L. Pothan, N. Cordeiro, M. Faria and S. Thomas, Biodegradable nanocomposite films based on sodium alginate and cellulose nanofibrils, *Materials*, 2016, **9**, 50, DOI: https://doi.org/10.3390/ma9010050.
58. A. K. Kesari, S. Mandava, C. K. Munagala, H. Nagar and V. Aniya, DES-ultrasonication processing for cellulose nanofiber and its compounding in biodegradable starch based packaging films through extrusion, *Ind. Crops Prod.*, 2022, **188**, 115566, DOI: https://doi.org/10.1016/j.indcrop.2022.115566.
59. T. S. M. Ribeiro, C. C. N. Martins, M. V. Scatolino, M. C. Dias, A. R. P. Mascarenhas, C. B. Ferreira, M. L. Bianchi and G. H. D. Tonoli, Using cellulose nanofibril from sugarcane bagasse as an eco-friendly ductile reinforcement in starch films for packaging, *Sustainability*, 2025, **17**, 4128, DOI: https://doi.org/10.3390/su17094128.
60. E. Gashawtena, A. Kidane and B. Sirahbizu, The effect of nanocellulose and silica filler on the mechanical properties of natural fiber polymer matrix composites, *Results Eng.*, 2024, **24**, 102898, DOI: https://doi.org/10.1016/j.rineng.2024.102898.
61. Y. Xu, Z. Wu, A. Li, N. Chen, J. Rao and Q. Zeng, Nanocellulose composite films in food packaging materials: a review, *Polymers*, 2024, **16**, 423, DOI: https://doi.org/10.3390/polym16030423.
62. M. Wakabayashi, S. Fujisawa, T. Saito and A. Isogai, Nanocellulose film properties tunable by controlling degree of fibrillation of TEMPO-oxidized cellulose, *Front. Chem.*, 2020, **8**, 37, DOI: https://doi.org/10.3389/fchem.2020.00037.
63. M. Hassan, L. Berglund, R. Abou-Zeid, E. Hassan, W. Abou-Elseoud and K. Oksman, Nanocomposite film based on cellulose acetate and lignin-rich rice straw nanofibers, *Materials*, 2019, **12**, 595, DOI: https://doi.org/10.3390/ma12040595.
64. H. Zhang, X. Tang, X. Gao and K. Chen, Fabrication and comparative evaluation of regenerated cellulose films using pulp fines and pith from corn stalk in DMAc/LiCl

solvent system, *BioResources*, 2019, **14**, 6421–6432, DOI: https://doi.org/10.15376/biores.14.3.6421-6432.

65. S. S. Shazleen, L. Y. Foong Ng, N. A. Ibrahim, M. A. Hassan and H. Ariffin, Combined effects of cellulose nanofiber nucleation and maleated polylactic acid compatibilization on the crystallization kinetic and mechanical properties of polylactic acid nanocomposite, *Polymers*, 2021, **13**, 3226, DOI: https://doi.org/10.3390/polym13193226.
66. R. Kose and T. Kondo, Size effects of cellulose nanofibers for enhancing the crystallization of poly(lactic acid), *J. Appl. Polym. Sci.*, 2013, **128**, 1200–1205, DOI: https://doi.org/10.1002/app.38308.
67. S. S. Shazleen, F. A. Sabaruddin, Y. Ando and H. Ariffin, Optimization of cellulose nanofiber loading and processing conditions during melt extrusion of poly(3-hydroxybutyrate-co-3-hydroxyhexanoate) bionanocomposites, *Polymers*, 2023, **15**, 671, DOI: https://doi.org/10.3390/polym15030671.
68. S. Roy, H. C. Kim, P. S. Panicker, J.-W. Rhim and J. Kim, Cellulose nanofiber-based nanocomposite films reinforced with zinc oxide nanorods and grapefruit seed extract, *Nanomaterials*, 2021, **11**, 877, DOI: https://doi.org/10.3390/nano11040877.
69. S. S. Lal and S. T. Mhaske, Old corrugated box (OCB)-based cellulose nanofiber-reinforced and citric acid-cross-linked TSP–guar gum composite film, *Polym. Bull.*, 2021, **78**, 885–915, DOI: https://doi.org/10.1007/s00289-020-03138-y.
70. C. Miao and W. Y. Hamad, In-situ polymerized cellulose nanocrystals (CNC)–poly(L-lactide) (PLLA) nanomaterials and applications in nanocomposite processing, *Carbohydr. Polym.*, 2016, **153**, 549–558, DOI: https://doi.org/10.1016/j.carbpol.2016.08.012.
71. M. R. Amri, C. T. Guan, S. S. Osman Al-Edrus, F. Md Yasin and S. F. Mohamad, Effect of cellulose nanofibrils on the properties of jatropha oil-based waterborne polyurethane nanocomposite film, *Polymers*, 2021, **13**, 1460, DOI: https://doi.org/10.3390/polym13091460.
72. A. González, G. Gastelú, G. N. Barrera, P. D. Ribotta and C. I. Álvarez Igarzabal, Preparation and characterization of soy protein films reinforced with cellulose nanofibers obtained from soybean by-products, *Food Hydrocolloids*, 2019, **89**, 758–764, DOI: https://doi.org/10.1016/j.foodhyd.2018.11.051.
73. S. Tanpichai, A. Boonmahitthisud, N. Soykeabkaew and L. Ongthip, Review of the recent developments in all-cellulose nanocomposites: properties and applications, *Carbohydr. Polym.*, 2022, **286**, 119192, DOI: https://doi.org/10.1016/j.carbpol.2022.119192.
74. B. Baghaei and M. Skrifvars, All-cellulose composites: a review of recent studies on structure, properties and applications, *Molecules*, 2020, **25**, 2836, DOI: https://doi.org/10.3390/molecules25122836.
75. J. Sun, X. Yang, Y. Bai, Z. Fang, S. Zhang, X. Wang, Y. Yang and Y. Guo, Recent advances in cellulose nanofiber modification and characterization and cellulose nanofiber-based films for eco-friendly active food packaging, *Foods*, 2024, **13**, 3999, DOI: https://doi.org/10.3390/foods13243999.
76. M. Wang, X. Miao, H. Li and C. Chen, Effect of length of cellulose nanofibers on mechanical reinforcement of polyvinyl alcohol, *Polymers*, 2021, **14**, 128, DOI: https://doi.org/10.3390/polym14010128.
77. H.-L. Nguyen, Z. Hanif, S.-A. Park, B. G. Choi, T. H. Tran, D. S. Hwang, J. Park, S. Y. Hwang and D. X. Oh, Sustainable boron nitride nanosheet-reinforced cellulose nanofiber composite film with oxygen barrier without the cost of color and cytotoxicity, *Polymers*, 2018, **10**, 501, DOI: https://doi.org/10.3390/polym10050501.

78. M. J. Gidado, A. A. N. Gunny, S. C. B. Gopinath, A. Ali, C. Wongs-Aree and N. H. M. Salleh, Challenges of postharvest water loss in fruits: mechanisms, influencing factors, and effective control strategies – a comprehensive review, *J. Agric. Food Res.*, 2024, **17**, 101249, DOI: https://doi.org/10.1016/j.jafr.2024.101249.
79. S. Yue, T. Zhang, S. Wang, D. Han, S. Huang, M. Xiao and Y. Meng, Recent progress of biodegradable polymer package materials: nanotechnology improving both oxygen and water vapor barrier performance, *Nanomaterials*, 2024, **14**, 338, DOI: https://doi.org/10.3390/nano14040338.
80. L. Amoroso, K.J. De France, N. Kummer, Q. Ren, G. Siqueira and G. Nyström, Nanocomposites of cellulose nanofibers incorporated with carvacrol via stabilizing octenyl succinic anhydride-modified ε-polylysine, *Int. J. Biol. Macromol.*, 2023, **242**, 124869, DOI: https://doi.org/10.1016/j.ijbiomac.2023.124869.
81. E. Rincón, J. De Haro-Niza, R. Morcillo-Martín, E. Espinosa and A. Rodríguez, Boosting functional properties of active-CMC films reinforced with agricultural residues-derived cellulose nanofibres, *RSC Adv.*, 2023, **13**, 24755–24766, DOI: https://doi.org/10.1039/D3RA04003H.
82. B. Zhang, C. Huang, H. Zhao, J. Wang, C. Yin, L. Zhang and Y. Zhao, Effects of cellulose nanocrystals and cellulose nanofibers on the structure and properties of polyhydroxybutyrate nanocomposites, *Polymers*, 2019, **11**, 2063, DOI: https://doi.org/10.3390/polym11122063.
83. Q.-H. Lu and F. Zheng, Polyimides for electronic applications, *in* Advanced Polyimide Materials, Elsevier, pp. 195–255, DOI: https://doi.org/10.1016/B978-0-12-812640-0.00005-6.
84. W. Kargupta, R. Seifert, M. Martinez, J. Olson, J. Tanner and W. Batchelor, Preparation and benchmarking of novel cellulose nanopaper, *Cellulose*, 2022, **29**, 4393–4411, DOI: https://doi.org/10.1007/s10570-022-04563-0.
85. M. Babin, G. C. Eder, Y. Voronko and G. Oreski, Water vapor permeability of polymeric packaging materials for novel glass-free photovoltaic applications, *J. Appl. Polym. Sci.*, 2024, **141**, e55733, DOI: https://doi.org/10.1002/app.55733.
86. E.-K. Uusi-Tarkka, M. Skrifvars and A. Haapala, Fabricating sustainable all-cellulose composites, *Appl. Sci.*, 2021, **11**, 10069, DOI: https://doi.org/10.3390/app112110069.
87. S. S. Ahankari, A. R. Subhedar, S. S. Bhadauria and A. Dufresne, Nanocellulose in food packaging: a review, *Carbohydr. Polym.*, 2021, **255**, 117479, DOI: https://doi.org/10.1016/j.carbpol.2020.117479.
88. E. Pasquier, B. D. Mattos, H. Koivula, A. Khakalo, M. N. Belgacem, O. J. Rojas and J. Bras, Multilayers of renewable nanostructured materials with high oxygen and water vapor barriers for food packaging, *ACS Appl. Mater. Interfaces*, 2022, **14**, 30236–30245, DOI: https://doi.org/10.1021/acsami.2c07579.
89. E. Jamróz, P. Kulawik and P. Kopel, The effect of nanofillers on the functional properties of biopolymer-based films: a review, *Polymers*, 2019, **11**, 675, DOI: https://doi.org/10.3390/polym11040675.
90. M. Alizadeh-Sani, A. Khezerlou and A. Ehsani, Fabrication and characterization of the bionanocomposite film based on whey protein biopolymer loaded with TiO_2 nanoparticles, cellulose nanofibers and rosemary essential oil, *Ind. Crops Prod.*, 2018, **124**, 300–315, DOI: https://doi.org/10.1016/j.indcrop.2018.08.001.
91. L. Wei, H. Bian, U. P. Agarwal, R. C. Sabo, L. M. Matuana and N. M. Stark, Correlation between morphology and performance of cellulose nanofibril-based films, *Curr. Res. Green Sustain. Chem.*, 2023, **6**, 100363, DOI: https://doi.org/10.1016/j.crgsc.2023.100363.
92. H. E. Cainglet, J. R. Black, H. Udugoda, N. Nasiri, G. L. Diaz-Arenas, G. Garnier, W. Batchelor and J. Tanner, Can pure cellulose nanofibril films replace polyolefins as

water vapor barriers in packaging?, *J. Colloid Interface Sci.*, 2025, **678**, 547–555, DOI: https://doi.org/10.1016/j.jcis.2024.09.060.
93. A. Dey and S. Neogi, Oxygen scavengers for food packaging applications: a review, *Trends Food Sci. Technol.*, 2019, **90**, 26–34, DOI: https://doi.org/10.1016/j.tifs.2019.05.013.
94. P. Gupta, Role of oxygen absorbers in food as packaging material, their characterization and applications, *J. Food Sci. Technol.*, 2024, **61**, 242–252, DOI: https://doi.org/10.1007/s13197-023-05681-8.
95. T. Ben Shalom, S. Belsey, M. Chasnitsky and O. Shoseyov, Cellulose nanocrystals and corn zein oxygen and water vapor barrier biocomposite films, *Nanomaterials*, 2021, **11**, 247, DOI: https://doi.org/10.3390/nano11010247.
96. A. I. Garba, Food preservation packaging, *in* Food Processing and Packaging Technologies – Recent Advances, IntechOpen, DOI: https://doi.org/10.5772/intechopen.110043.
97. M. R. Miah, J. Ding, H. Zhao, H. Wang, Q. Chu, B. Fang, L. Fan, J. Wang and J. Zhu, Enhancing the mechanical and barrier properties of biobased polyester incorporated with carboxylated cellulose nanofibers, *Mater. Today Commun.*, 2024, **38**, 108538, DOI: https://doi.org/10.1016/j.mtcomm.2024.108538
98. M. Mazaheri, J. T. Kim and G. H. Shin, Synergistic enhancement of PLA/PHA bio-based films using TEMPO-oxidized cellulose nanofibers, graphene oxide, and clove oil for sustainable packaging, *Mater. Today Commun.*, 2025, **42**, 111531, DOI: https://doi.org/10.1016/j.mtcomm.2025.111531.
99. A. H. Tayeb, M. Tajvidi and D. Bousfield, Enhancing the oxygen barrier properties of nanocellulose at high humidity: numerical and experimental assessment, *Sustain. Chem.*, 2020, **1**, 198–208, DOI: https://doi.org/10.3390/suschem1030014.
100. G. Chinga-Carrasco and K. Syverud, On the structure and oxygen transmission rate of biodegradable cellulose nanobarriers, *Nanoscale Res. Lett.*, 2012, **7**, 192, DOI: https://doi.org/10.1186/1556-276X-7-192.
101. L. Alves, A. Ramos, E. Ferraz, P. J. T. Ferreira, M. G. Rasteiro and J. A. F. Gamelas, Design of cellulose nanofibre-based composites with high barrier properties, *Cellulose*, 2023, **30**, 10157–10174, DOI: https://doi.org/10.1007/s10570-023-05495-z.
102. S. Jali, T. P. Mohan, F. M. Mwangi and K. Kanny, A review on barrier properties of cellulose/clay nanocomposite polymers for packaging applications, *Polymers*, 2023, **16**, 51, DOI: https://doi.org/10.3390/polym16010051.
103. M. Hubbe and W. Grigsby, From nanocellulose to wood particles: a review of particle size vs. the properties of plastic composites reinforced with cellulose-based entities, *BioResources*, 2020, **15**, 2030–2081, DOI: https://doi.org/10.15376/biores.15.1.2030-2081.
104. G. G. De Lima, I. C. B. Zakaluk, M. A. Artner, A. C. Pedro, P. H. Gonzalez De Cademartori, G. I. B. D. Muniz and W. L. E. Magalhães, Enhancing barrier and antioxidant properties of nanocellulose films for coatings and active packaging: a review, *ACS Appl. Nano Mater.*, 2025, **8**, 4397–4421, DOI: https://doi.org/10.1021/acsanm.4c04805.
105. Y. Xu, Z. Wu, A. Li, N. Chen, J. Rao and Q. Zeng, Nanocellulose composite films in food packaging materials: a review, *Polymers*, 2024, **16**, 423, DOI: https://doi.org/10.3390/polym16030423.
106. J. Wang, D. J. Gardner, N. M. Stark, D. W. Bousfield, M. Tajvidi and Z. Cai, Moisture and oxygen barrier properties of cellulose nanomaterial-based films, *ACS Sustainable Chem. Eng.*, 2018, **6**, 49–70, DOI: https://doi.org/10.1021/acssuschemeng.7b03523.
107. S. Belbekhouche, J. Bras, G. Siqueira, C. Chappey, L. Lebrun, B. Khelifi, S. Marais and A. Dufresne, Water sorption behavior and gas barrier properties of cellulose

whiskers and microfibrils films, *Carbohydr. Polym.*, 2011, **83**, 1740–1748, DOI: https://doi.org/10.1016/j.carbpol.2010.10.036.

108. S. S. Nair, J. Zhu, Y. Deng and A. J. Ragauskas, High performance green barriers based on nanocellulose, *Sustain. Chem. Process.*, 2014, **2**, 23, DOI: https://doi.org/10.1186/s40508-014-0023-0.
109. D. Dag, J. Jung and Y. Zhao, Development and characterization of cellulose nanofiber reinforced hydroxypropyl methylcellulose films functionalized with propolis-loaded zein nanoparticles and its application for cheddar cheese storage, *Int. J. Biol. Macromol.*, 2024, **261**, 129790, DOI: https://doi.org/10.1016/j.ijbiomac.2024.129790.
110. Z. Fan, Y. Hao, Y. Wang, X. Hu and T. Li, Characterisation of hyaluronic acid–curcumin–cellulose nanofibre composite film and application in egg preservation, *Int. J. Food Sci. Technol.*, 2023, **58**, 6263–6271, DOI: https://doi.org/10.1111/ijfs.16729.
111. H. Mohammadi, M. Rezaeigolestani and M. Mohsenzadeh, Optimization of antimicrobial nanocomposite films based on carboxymethyl cellulose incorporating chitosan nanofibers and guggul gum polysaccharide, *Sci. Rep.*, 2024, **14**, 13693, DOI: https://doi.org/10.1038/s41598-024-64528-0.
112. S. Malarat, D. Khongpun, K. Limtong, N. Sinthuwong, P. Soontornapaluk, C. Sakdaronnarong and P. Posoknistakul, Preparation of nanocellulose from coffee pulp and its potential as a polymer reinforcement, *ACS Omega*, 2023, **8**, 25122–25133, DOI: https://doi.org/10.1021/acsomega.3c02016.
113. P.G. Gan, S.T. Sam, M.F.B. Abdullah and M.F. Omar, Thermal properties of nanocellulose-reinforced composites: a review, *J. Appl. Polym. Sci.*, 2020, **137**, 48544, DOI: https://doi.org/10.1002/app.48544.
114. M. Manimaran, M. N. Norizan, M.H.M. Kassim, M. R. Adam, M. N. F. Norrrahim and V. F. Knight, Critical assessment of the thermal stability and degradation of chemically functionalized nanocellulose-based polymer nanocomposites, *Nanotechnol. Rev.*, 2024, **13**, 20240005, DOI: https://doi.org/10.1515/ntrev-2024-0005.
115. R. G. Ramírez Brenes, L.D.S. Chaves, N. Bojorge and N. Pereira, Endo-exoglucanase synergism for cellulose nanofibril production assessment and characterization, *Molecules*, 2023, **28**, 948, DOI: https://doi.org/10.3390/molecules28030948.
116. A.C.F. Louis, S. Venkatachalam and S. Gupta, Innovative strategy for rice straw valorization into nanocellulose and nanohemicellulose and its application, *Ind. Crops Prod.*, 2022, **179**, 114695, DOI: https://doi.org/10.1016/j.indcrop.2022.114695.

View Article Online
DOI: 10.1039/D6FB00014B

Data Availability Statement

The data that support the findings of this study are available from the corresponding author upon reasonable request.